NANOscientific

VOL 23 WINTER 2022

The Magazine for NanoScience and Technology

# Park Systems Special Edition

Park Systems unveils the inner workings of the new Park FX40



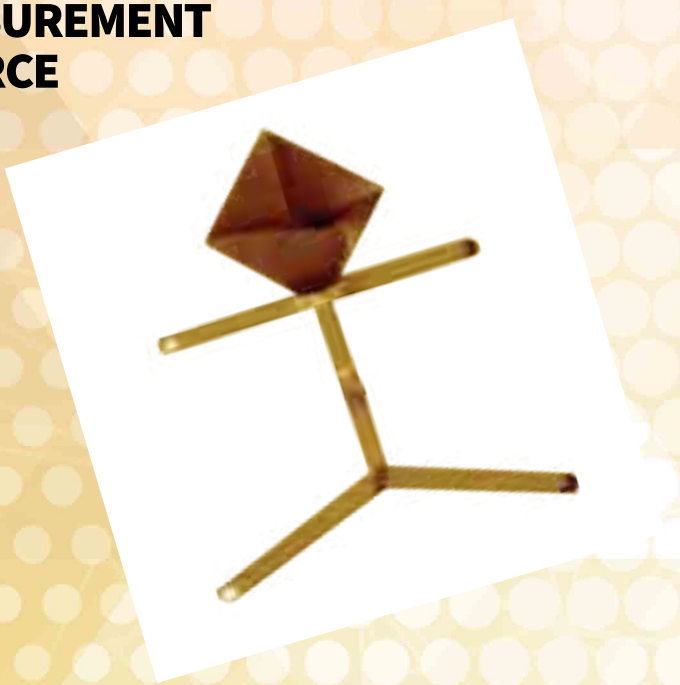

NANOscientific

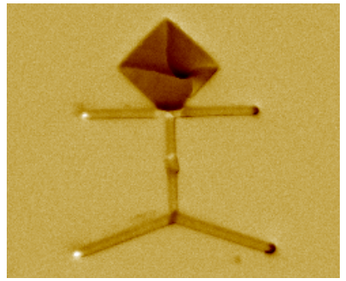

*Micro man Pattern on Ta/NiFe/Ta in MFM mode provided by Prof. Lew Wen Siang, NTU SPMS, Singapore provided by Prof. Lew Wen Siang, School of Physical and Mathematical Sciences, Nanyang Technological University (NTU), Singapore*

We enjoy hearing from you, our readers.
Send your research or story ideas to
**debbie@nanoscientific.org**

To view all of our articles,
please visit our web site at
**www.nanoscientific.org**



Park SYSTEMS
Park Systems Corp.
KANC 15F, Gwanggyo-ro 109,
Suwon 16229, Korea
inquiry@parksystems.com
**www.parkystems.com**

# Contents



# LETTER FROM DR. PARK

CEO PARK SYSTEMS AND FIRST TO COMMERCIALIZE AFM

**Greetings!**
We are about to bid adieu to 2021 that has been a very difficult year for everyone caused by the coronavirus. I sincerely hope this letter finds you well in good health and in good spirit.

I am happy to report that thanks to your continued support and best wishes, we were able to achieve many great initiatives this year. We have been expanding the AFM business through diligent engineering development, introducing new innovative products including the Park FX40, and actively executing global marketing strategies. Through continuous delivery of good financial results and showing favorable future growth potential, we surpassed the 1 trillion KRW market capitalization at one time. With the fast growing market cap of our company, Park Systems is now listed in the KOSDAQ 150 index and KRX300 index—the underlying index for financial instruments and ETFs, and the leading benchmark of the Korean stock market representing 300 sector leaders in the KOSPI and KOSDAQ markets, respectively.

We were fortunate to recruit many accomplished executive-level managers this year, and we have restructured the management to allow existing executives to take on bigger and more suitable roles.

Furthermore, we established the Park Mini-MBA program led by Hanyang University faculty, as part of the middle management education. This has been very effective and well received by the managers.

Our company was selected as the KOSDAQ Rising Star for four consecutive years. Furthermore, I was awarded the 'Korea Hidden Champion Award' from The Korean Academic Society of Business Administration.
In addition, Park Systems was named in the '2021 Korea IR Grand Prize-IR Excellent Company' by the Korea IR Council for the preeminence in investor relations. The Korea IR Council selects the top 20 out of 2,300 publicly traded companies each year.

As we look back over this passing year, we would like to express our sincere gratitude to all of you who have supported and helped us continue to grow and prosper. We promise to repay your expectations with our continued commitment to excellence and hard work in the new year 2022. Happy New Year and I wish you all the best for you and your loved ones.

**Yours truly,**
**Sang-il Park, Ph.D.**
Chairman& CEO
Park Systems Corporation
December 2021


As we enter 2022, NanoScientific shares with you the peace and joy of the season, guided by the knowledge that our global footprint covers every continent and binds us to the SPM community. With the frontiers of Nanotechnology rapidly advancing society's future, nanometrology is at the forefront of exciting and uplifting ways to support progress and improve society. The virtual world has created an atmosphere where scientific minds can seamlessly work together to solve life's most pressing questions. In the spirit of a better world and a brighter future, we are proud to present the Winter Edition of NanoScientific.

This issue is filled with exciting articles highlighting the progress AFM has made since the beginning of the Nanotechnology Revolution. Now nanotechnology has fully integrated into industries both consumer and industrial. The view that scientists see displays the subatomic actions from particles we have never seen before. From this quantum knowledge, we learn that particles interact in a connected and unified field in multiple spheres of existence.

As the new year unfolds, we eagerly await discoveries that connect the quantum world of matter to the unseen world that binds it together. This issue highlights nanometrology tools that are more automated and infused with new technologies that allow scientists to easily adapt to the fast-paced environment of scientific discovery we are all witnessing.

As always, please share with us any story ideas or suggestions for topics and enjoy a prosperous and light filled New Year.

From all of us at

NANOscientific

# NANOMECHANICAL PROPERTIES OF LIPID VESICLES USING ATOMIC FORCE MICROSCOPY

Park SYSTEMS

Gabriela Mendoza, Ph.D., Park Systems Mexico

## Introduction

The unique structures of liposomes – lipid vesicles (spherical structures with a bilayer membrane) of varying size and structural complexities within other lipid vesicles – have been utilized to serve as a drug delivery mechanism over an extended period of time [1]. In this study, a Park NX10 Atomic Force Microscope (AFM) is used to differentiate organic material from a substrate using True Non-Contact™ and Tapping, and to quantify nanomechanical properties using PinPoint™ Mode.

Biological membranes define cell boundaries as well as any cell compartment. To some extent, the functionality of membranes is related to the elastic properties of the lipid bilayer and the mechanical and hydrophobic matching with functional membrane proteins. In general, membrane dimensions and mechanical properties (i.e. bilayer thickness, bending and stretching stiffness/membrane tension) modify the function of any membrane protein [2].

AFM is an ideal technique for studying both topographical and nanomechanical characteristics of lipid vesicles on a highly localized level. That is because AFM can generate unique, high-resolution images of biological and organic samples with little or no sample preparation [3].

## Experimental

Phospholipid vesicles were prepared by co-solubilization and were composed of a 1:1 ratio of 1,2-Dipalmitoyl-sn glycero-3-phosphocholine (DPPC) and 1,2-dipalmitoyl-sn-glycero-3-phosphoethanolamine (DPPE) as well as a Na,K-ATPase enzyme that maintained a phospholipid to protein ratio of 1:3 (w/w). The sample was dispersed onto a mica substrate and placed into a metal sample holder.

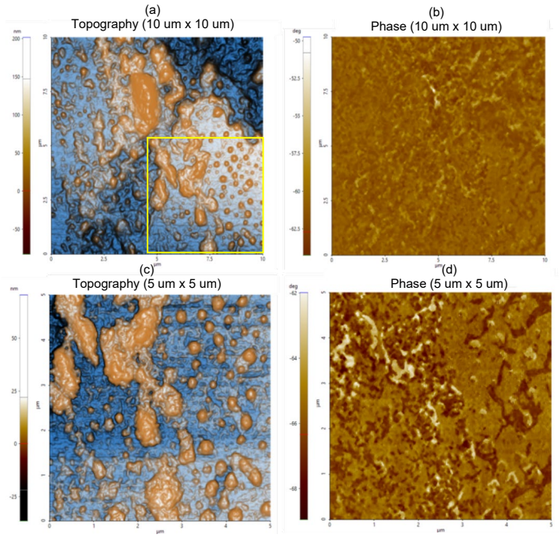


*Figure 1. Non-contact (a) topography and (b) phase AFM images. Scan Size: 10 µm x 10 µm, Image size: 256 pixels x 256 pixels. Magnified view of (c) topography and (d) phase inside the yellow box in Figure 1a. Scan size: 5 µm x 5 µm, image size: 256 pixels x 256 pixels. .*

Experiments were conducted with an NX10 AFM under ambient conditions using an active anti-vibration stage and acoustic enclosure using a Force Modulation Mode (FMR) cantilever (2N/m). Topography, adhesion energy and modulus images were acquired using PinPointTM Nanomechanical Mode.

## Results and Discussion

Figure 1a depicts the topography and phase images revealing particle of varying sizes. The smaller individual particles correspond to lipid vesicles and larger particles correspond to giant lipid vesicles and/or agglomerates. The yellow square highlights the scan area of subsequent images shown in Figure 1c. The phase image shown in figure 1b reveals that the sample was homogeneously distributed over the substrate.

The dimensions of those particles identified in 1c are in the range of hundreds of nm in length (refer to Figure 2 for the detailed analysis). The phase image (Figure 1d) allows distinction of particles and agglomerates from the substrate sample, mica in this case.

The three selected vesicles in Figure 2a were measured. Figures 2b, 2c and 2d show the line profiles for vesicles marked by the green, blue and red lines, respectively.

Their dimensions are 200 µm long by 26 µm high (blue), 208 µm long by 22 µm high (green) and 183 µm long by 29 µm high (red).

Topography, adhesion energy and modulus were simultaneously acquired during a single scan in PinPoint. Figure 3 shows the (a) topography, (b) adhesion energy and (c) modulus images taken. Line profiles along topography (red), adhesion energy (green) and modulus (blue) are shown as well. Figure 3d summarizes the quantitative results of the line profiles (Figures 3a-c). From 110 nm to 400 nm, measurements correspond to the selected lipid vesicle from the blue rectangle. From 400 nm to 600 nm, it corresponds to the substrate.



From the adhesion energy image (green line), higher values are observed for lipid vesicles compared with the substrate. The modulus on the lipid vesicle) is, as expected, smaller than that of the substrate.

A higher resolution modulus dataset is shown in Figure 4. Three areas within that image were selected to measure the modulus of individual particles. Those lipid vesicles were selected because of their defined shape. The module values for the selected vesicles are 78.05 MPa, 86.05 MPa and 78.80 MPa for the red, green and blue dotted circles, respectively.
There are two peaks that were detected in the modulus image histogram. One is ~86 MPa and the other is ~110 MPa. One of these values corresponds to lipid vesicles and the other to a relatively harder substrate. The modulus value differs from reported literature values (approximately 30 MPa) [4], and it is likely due to prolonged exposure to air that caused the hardening.

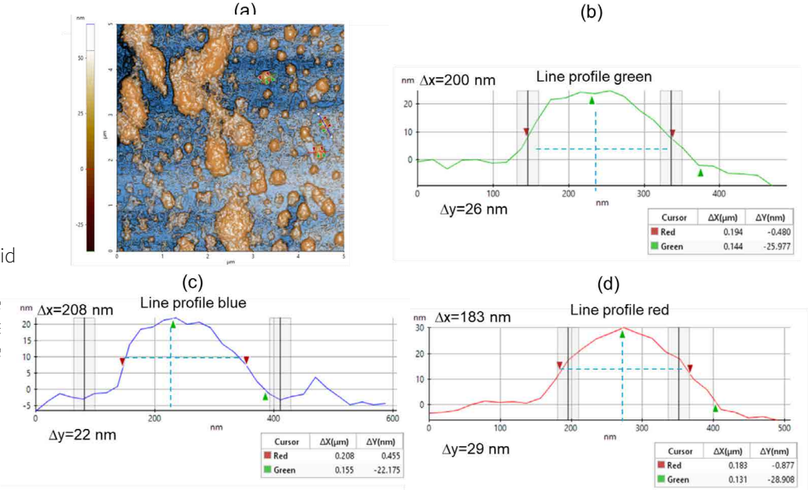


*Figure 2. Topography images and line profile analyses: (a) Non-contact topography AFM image – scan size: 5 µm x 5 µm, image size: 256 pixels x 256 pixels; (b-d) Corresponding line profiles from Figure 2a.*

## Conclusions

Visualizing, measuring, and understanding the mechanical properties of biological and organic samples such as lipid vesicles on the nanoscale is important for understanding their function and uses. This study demonstrates that Atomic Force Microscopy (AFM) can provide that information to the researcher with high precision and resolution. Specifically, this paper shows that an AFM can reliably generate nanoscale topography of lipid and acquire the modulus of the sample with high precision using Park's PinPoint Mode.

## References

[1] Suzuki S., and Gerner P. (2013), Pharmacology and Physiology for Anesthesia, Elsevier, Inc.
[2] Picas L., Rico F., Scheuring S., Direct Measurement of the Mechanical Properties of Lipid Phases in Supported Bilayers. Biophysical Journal. Volume 102(1), 2012.
[3] AFM Imaging as a Tool to Visualize Bilayer Formation from Lipid Vesicles. Retrieved from https://www.parksystems.com/images/applications/biological/note/AN-R05.pdf
[4] Sebinelli H. G., Borin I. A., Ciancaglini P., and Bolean M., Topographical and mechanical properties of liposome surfaces harboring Na,K ATPase by means of atomic force microscopy. Soft Matter 15, 2737, 2019.

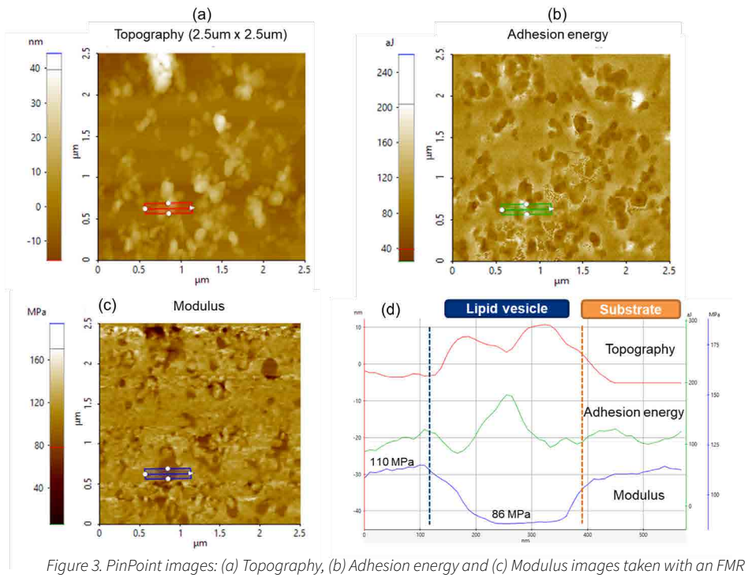


*Figure 3. PinPoint images: (a) Topography, (b) Adhesion energy and (c) Modulus images taken with an FMR cantilever; (d) Corresponding adhesion energy and modulus line profiles are shown in the bottom right panel.*

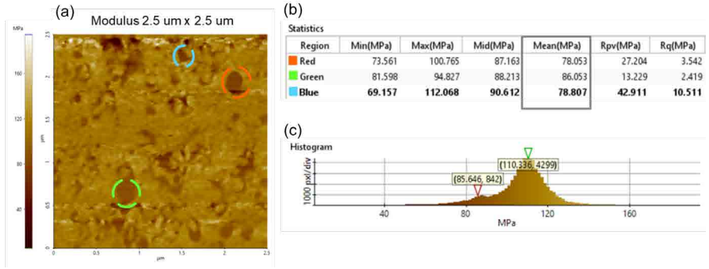


*Figure 4. Modulus analysis obtained using the PinPoint Mode: (a) Modulus image – scan size 2.5 µm x 2.5 µm, image size: 256 pixels x 256 pixels; (b) Statistics obtained with Park XEI software of the red, green and blue dotted circles statistics in Figure 4a; (c) Modulus image histogram showing the two peaks detected.*

# DESIGNING A NEW CLASS OF ATOMIC FORCE MICROSCOPE – PARK FX40 THE AUTOMATIC AFM

Ryan YK Yoo, Ph.D., Park Systems

*Left: Front view of Park FX40. Below: From XE to FX: Park Systems AFM product line has undergone a major renewal every decade.*

## Product Line Renewal Every Decade

A decade is sufficient for market disruption and adaptation in Atomic Force Microscope (AFM) industry. Park Systems Corp. (Park), a manufacturer of AFM, has introduced a new major platform every 10 years. Features and capabilities of the first product foretell the product and business strategy of coming decade. Building on the crosstalk elimination design of the XE-series AFMs, Park tapped into the industrial automation market and entered the hard disk market. With the lower noise design of the NX-series AFM, accurate measurement data on large samples became possible, and Park entered the semiconductor industry. Our goal with the groundbreaking user interface in AFM automation, is that the FX product line will enable a new breed of AFM solutions to capture opportunities of major stake against established microscopy industries such as electron or optical microscopes.

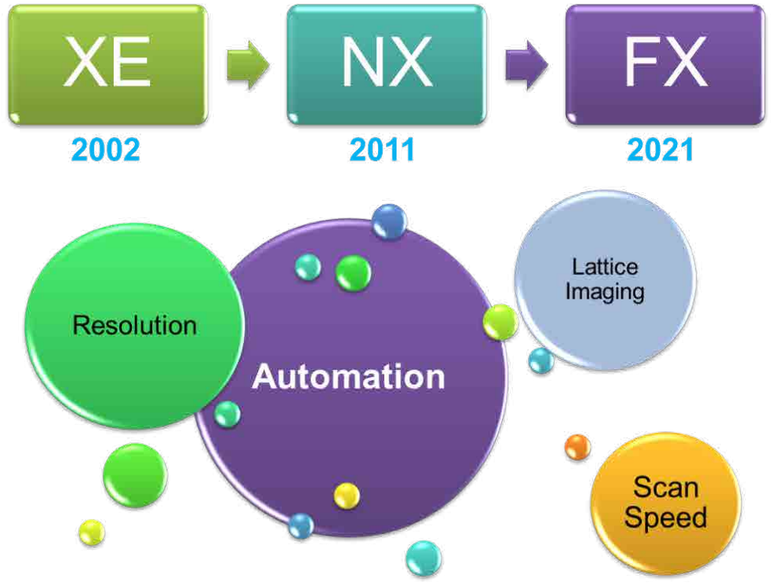


*Figure 2. How Park will contribute to market conversation of AFM industry. Automation is a major central theme in Park's R&D efforts, followed by system performance in resolution. Other agenda such as lattice imaging and scan speed are considered for specific sample and measurement needs.*

## Is AFM Easy to Use?

The purpose of AFM is to measure surface topography and other physical properties repeatedly and reliably in three dimensions with sub-nanometer resolution. Sample preparation is minimal, if any, and cost of ownership is low compared to related techniques. This has made AFMs indispensable tools in industrial and research applications. However, wide scale acceptance of AFM was previously hampered by complex operation and handling. Although commercial AFMs have been improved over time, AFM is still difficult to learn and operate for many prospective new users with no prior experience.

Traditionally, AFM operation required manual input and setup from the researcher. Before obtaining any AFM data, a user must select a suitable probe, load it into the AFM system often using tweezers, and align the optical detection system and viewing optics. This is followed by loading a sample and selecting one or more areas to image and analyze. The user then must select an imaging mode, tune the system, and guide the AFM tip to within detection range of the surface. To obtain valid surface information, the user must tell the AFM how to track the sample surface. These rather complex procedures have prevented AFM from entering mainstream as it generally takes a very experienced person to obtain good, reproducible data.

Enhanced user convenience and higher performance can be the two differentiating benefits that may justify Park's new product line. Enhanced user convenience primarily constitutes motorized and automated steps of tool operation. Higher performance, on the other hand, would imply better specification or additional capabilities of a given tool function to the justified and demonstrated benefit of a user. While AFM makers are competing on resolution, scan speed, or even lattice imaging, Park recognizes automation as the key request for AFM, which will disrupt and grow the market.

## FX: The Dream Machine Project

Park FX40 AFM was the dream machine project with the goals to maximize user convenience while adding features and increasing performance. For user convenience, full automation of probe exchange, beam alignment, and sample positioning were targeted from the very early stage of product design.

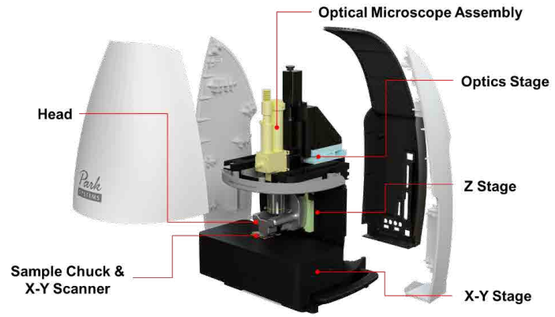


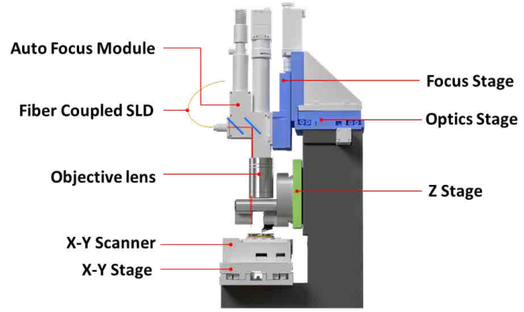


*Figure 3. Front view of Park FX40. The view on the right reveals some major components normally hidden by the microscope housing. Figure 4. The Optical Microscope Assembly is decoupled from the moving plate of Z stage, reducing total Z-stage mass. Fiber coupled SLD is attached to the Optical Microscope Assembly. SLD beam is focused through objective lens and always fixed at the center of optical vision.*

Performance-wise, system noise floor, servo performance, and optical vision were further optimized from previous engineering platforms.

Park FX40 was developed based on the experience gained using crosstalk elimination on the previous generation of Park AFMs [1]. The systems utilize two dedicated, fully independent, flexure scanners, one for sample (XY) and the other for probe (Z) movement. The raw out-of-plane-motion (OPM) before image correction is less than 2nm over 80mm scan range, enabling precise measurements without being impacted by common leveling artifacts. Proven successful in the previous NX- or XE-series, the Optical Microscope Assembly of Park FX40 is positioned in the center of the system. The AFM head is positioned along the center-axis of the Optical Microscope Assembly and moves with the Z stage. The sample chuck and the XY scanner on the XY stage are positioned right below the AFM head.

The Optical Microscope Assembly is attached to the focus stage and can move vertically. Unlike the existing NX-series AFM system, the focus stage is not attached to the Z stage but rides on a separate optics stage. This arrangement reduces the weight on the Z stage, increasing system stability and immunity to external vibrations. In combination with a sturdier Z stage built on a high stiffness cross-roller guide and two bearing blocks, the Park FX40 achieves a lower mechanical noise floor than the previous NX-series and XE-series AFM systems. Additionally, the optics stage moves the optical microscope assembly in XY plane, a design consideration important for AFM automation.

The main components of the Optical Microscope Assembly are the same as prior XE- and NX- generations: objective lens, tube lens, camera, and LED light source for vision. The difference is a fiber-coupled super-luminescent diode (SLD) which is attached on the side port of the Optical Microscope Assembly. The SLD beam is focused by the objective lens onto the AFM cantilever and is always fixed at the center of optical vision. The objective lens enables the FX40 to generate a very small target beam spot size enabling the use of a wide range of cantilever sizes and applications.

Optical vison quality, an important aspect of industrial automation, was improved compared to the NX-series AFMs. In the FX AFM head design, all obstructing elements, such as beam splitter, present in the previous designs were eliminated to optimize the optical beam path. Line pairs with width less than 1 μm can be resolved in optical vision of Park FX40.

## New FX Features

Park FX40 has the most advanced AFM design and interfaces for user convenience. High-level automation is the central design consideration that includes automatic probe exchange and SLD beam alignment with a click of button using pattern recognition. Inside FX40, there are three camera modules: 1) a main view camera at the system center, 2) a sample view camera on the left side of the system, and 3) a QR code reader on the right side. On the right side of the XY stage, there is the automatic tip exchanger (ATX) module that can hold up to 8 AFM probes. A sliding protective cover prevents foreign objects from dropping into the ATX module when it is not in use.

## Probe Loading

Probe loading has been viewed as the biggest barrier for entry users of AFM. The NX- or XE-series AFM systems addressed some of the challenge by using pre-mounted tips [2]. In Park FX40, new probes can be easily and safely mounted at once using an 8-probe cassette. Once the probe cassette is loaded onto the ATX, the probes are ready for automatic probe exchange by the AFM head. Individual probes can be also replaced manually and mounted onto a probehand by the user, just like in the XE and NX series of AFM.

SLD beam focused on PPP-NCHR

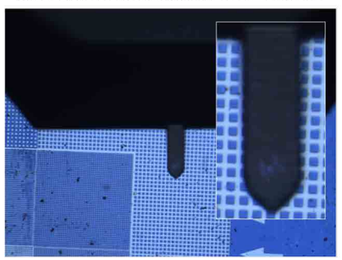

Vision from FX Optics

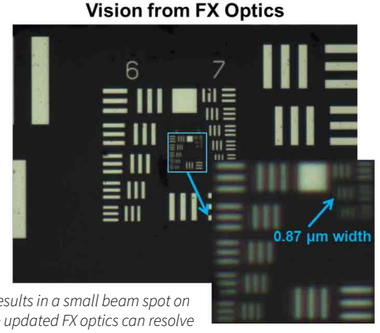


*Figure 5. Focusing the SLD beam through objective lens results in a small beam spot on the back of the cantilever for improved performance. The updated FX optics can resolve 0.87 μm linewidth.*

## Probe Exchange

In similar fashion to the automatic probe exchange on Park's industrial inline AFMs, probes are picked up by a magnetic force control mechanism [3]. The QR code reader recognizes the probe ID and the status of ATX slots. A vision recognition-based machine learning algorithm automatically detects whether probes are loaded onto their correct positions of the designated probe slots and generates a status report if there is an error during probe loading. The machine learning algorithm analyzes and weighs several factors, such as the shape of Park's patented chip carrier and loading position, to control and monitor successful or unsuccessful routines that results in improved loading success rates over time.

The QR code imprinted on the chip carrier of the probes holds information for probe identification such as probe type and serial number. With these information, the physical probe properties such as resonant frequency, spring constant, quality factor, cantilever geometry, tip geometry, drive percentages can be accessed from a database

Once the probes have been identified, the operator can select a probe to use and Park FX40 automatically picks a probe from the cassette. After that, the FX40 locates the cantilever and super-luminescent diode (SLD), and photodetector alignment are performed in a fully automatic fashion.

## Beam Alignment

In Park's new automated beam alignment, SLD beam position is automatically aligned for accurate and proper location onto a cantilever. The SLD is attached to the optical microscope assembly and the SLD beam is always fixed at the center of optical microscope. By using XY motor adjustments of the optics stage, the cantilever can be positioned at the center of optical vision image which automatically aligns the SLD beam to the cantilever. Based on the machine learning of a probe pattern, position of a probe is found by vision recognition.

The SLD beam emerging from the objective lens is focused onto the cantilever and reflected by a steering mirror. To complete the beam-bounce alignment, two motors inside the FX AFM head adjust the angle of the SLD beam

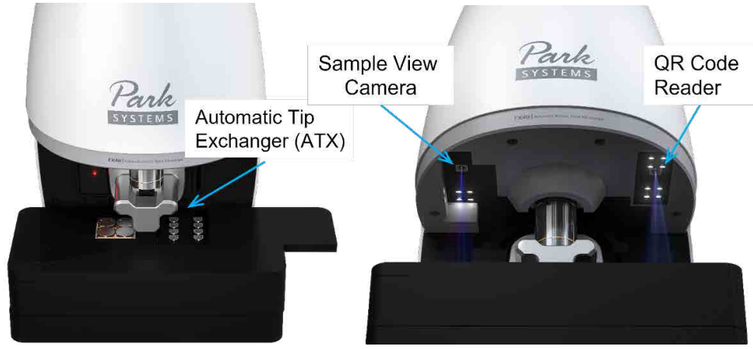


*Figure 6. The main components of the FX40 system include the ATX module shown on the right and three camera modules for main view at the center, a wide-angle sample view, and QR code reader.*


*Figure 7. Probe cassette exchange is done by placing an 8-probe cassette on the top of the ATX module and unscrewing the knob of the cassette cover.*

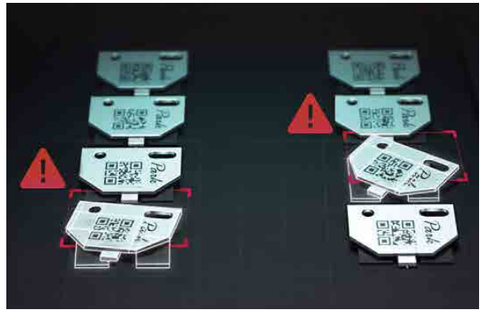

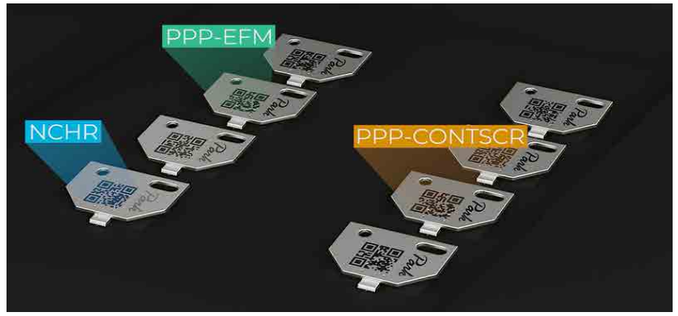


*Figure 9. The QR code reader identifies the probe type by reading the QR-codes on the chip carriers in the probe cassette.*

to the cantilever. Based on the machine learning of a probe pattern, position of a probe is found by vision recognition.

The SLD beam emerging from the objective lens is focused onto the cantilever and reflected by a steering mirror. To complete the beam-bounce alignment, two motors inside the FX AFM head adjust the angle of the SLD beam steering mirror, to aim the SLD beam onto the optimal location on the position-sensitive photodetector (PSPD). This automation eliminates user error during complex beam alignment process and ensures perfect alignment every time.

## Sample Navigation

The FX40 system comes with a Multi Snap-in Sample Chuck standard. Users can populate four sample plates that are kinematically mounted. The positioning repeatability of the sample disks is 5 µm in both X and Y. Using the four sample plates with repeatable positioning, one can make easy comparison between reference and target samples, e.g., KPFM work function, SCM dopant concentration, PinPointTM nanomechanical, or SThM thermal measurements.

The FX40 system uses a low-magnification sample view camera to aid the operator navigating to the desired imaging location. As the user clicks on the optical view screen, the XY stage coordinate of the clicked position is recognized, and the XY stage moves to locate the desired measurement directly underneath the probe tip.

For fine navigation the high-resolution optical view from the on-axis main view camera can be used. After sample navigation is completed, the cantilever then automatically approaches at the selected sample location. The sample height is measured by a new auto focus module for fast and quick engagement to sample surface. The tip approach is aided by carefully monitoring the effect of air damping while the probe is approaching the sample surface. The cantilever's vibration amplitude decreases monotonically and then linearly until the interatomic force will pull the tip to the surface at a threshold distance. This air damping effect can be used for automatic tip approach to ensure a fast but gentle tip-sample approach.

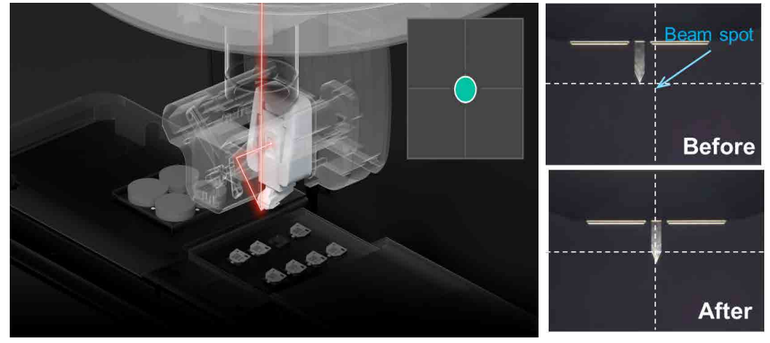


*Figure 10. Due to the fixed position of the SLD, centering the cantilever in the middle of the optics immediately aligns the SLD.*

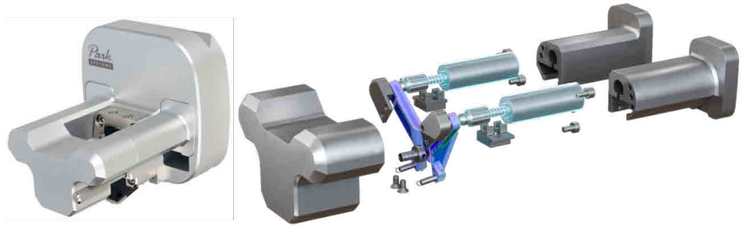

*Figure 11. New motorized FX AFM head optimizes the SLD beam spot position on the PSPD both vertically and laterally for optimal operation.*

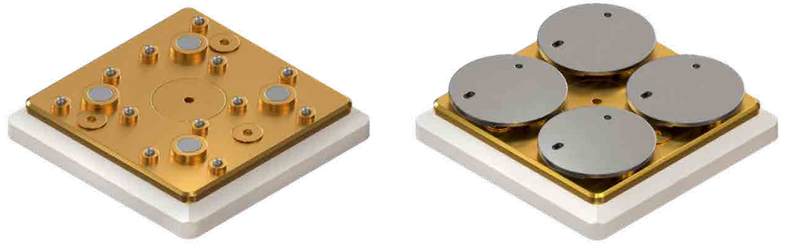

*Figure 12. Multi Snap-in Sample Chuck is a default sample chuck for Park FX40. The disks are kinematically mounted to ensure good mounting repeatability.*


*Figure 13. Sample navigation is made much easier by default off-axis sample view camera and fast moving XY stage. The picture on the left indicates the physical location of the camera while the right picture depicts an actual screen shot.*

## Imaging

SmartScanTM is a user-friendly interface that automates the whole imaging process and can help select imaging parameters based on objective boundary conditions and settings. It performs all the necessary imaging operations and intelligently selects the optimum image quality and scan speed [4]. This ensures consistent data quality independent of operator experience level. Processes such as the cantilever frequency sweep, operations setpoint, scan speed, or gain adjustment are part of the automatized procedures [5], reducing the time otherwise needed for manual user inputs and manipulation. Figure 15 shows the high-quality topography obtained using an NCHR cantilever, which clearly reveals Moiré patterns information of graphene on h-BN.

After completing data acquisition, the software secures the system by lifting the Z stage and turning the SLD off. The used probe returns to the ATX cassette if the operator does not plan to use it right away.

## Other FX Features

There are additional innovative features of Park FX40 to improve operation safety and servicing of AFM. Multiple integrated sensors measure essential environmental conditions such as temperature, humidity, sound, light, leveling and vibration near the system. The measured environmental conditions are displayed in SmartScanTM and stored in the image data, allowing the comparison of scanned images with different environmental conditions. This will provide additional environmental indicators to both users and customer service personnel.

Lastly, a new and revamped head crash prevention has been developed to protect probe and AFM scanner. A dedicated circuit monitors beam deflection and Z-detector signals in real time. Safety intervention by the circuit, algorithmically programmed, provides complete protection of the AFM, the most advanced of its kind.

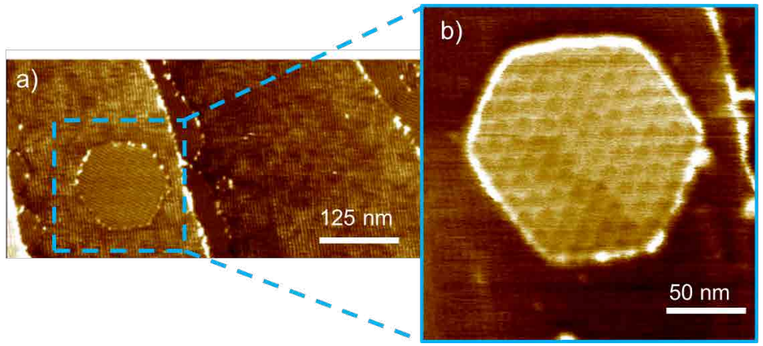


*Figure 14. Moiré pattern observed on graphene on h-BN. a) Topography scan of graphene on h-BN, vertical scale 0 to 6 nm. b) Zoom in: Moiré pattern clearly visible, vertical scale 0 to 6 nm.*

## Summary

Park renews its product line every 10 years with a new platform, and the features and capabilities of the first product foretell the product and business strategy of the coming decade. AFM is still difficult to learn and operate for many prospective new users. Park FX40 is a new generation, research-grade, automatic AFM platform with fully automated probe exchange and beam alignment, utilizing machine-learning technology overcoming these challenges. With easy sample navigation and an intelligent scan algorithm, Park FX40 further improves performance and productivity that is now accessible to everyone, experienced and new users alike. With the Park FX40, high-definition and meaningful data can be obtained with just a few clicks.


## Acknowledgement

The author wants to thank Dr. Stefan Kaemmer and Dr. Gilbert Min of Park Systems Americas for proofreading and editing the article, Rachel Bang for preparing the list of patents and publication, Kenneth Kang for the figures and schematics, and lastly Dr. Sang-il Park, founder and CEO of Park Systems Corp., for his technology vision and generous comments and feedback during product development and launch preparation of Park FX40.


## References


Joonhyung Kwon, Jaewan Hong, Yong-Seok Kim, Dong-Youn Lee, Kyumin Lee, Sang-min Lee, and Sang-il Park, “Atomic force microscope with improved scan accuracy, scan speed, and optical vision”, Rev. Sci. Instrum. 74, 4378 (2003).
US 6,945,100 B2 – Scanning probe microscope with improved probe tip mount – Sep.20,2005
US 8,099,793 B2 – Scanning probe microscope with automatic probe replacement function – Jan.17,2012
US 9,645,169 B2 – Measurement apparatus and method with adaptive scan rate – May.9,2017
US 10,133,052 – Image acquiring method and image acquiring apparatus using the sample – Nov.20,2018



*Figure 15. Various sensors monitor environmental conditions of AFM measurement such as temperature, humidity, and vibration.*



# QUANTITATIVE FRICTIONAL PROPERTIES MEASUREMENT USING ATOMIC FORCE MICROSCOPY


## Research Application Technology Center, Park Systems


## Introduction

Atomic force microscopy (AFM) is a powerful tool that can be used to obtain information on surface morphology of target materials in correlation with their frictional, electrical, mechanical, and thermal properties at the nano-scale. In particular, Lateral force microscopy (LFM) is an AFM technique that allows studying of the frictional properties quantitatively. Using LFM, friction information can be collected at various operational and experimental conditions (e.g., applied force, velocity, temperature, humidity, and vacuum). Hence, LFM can provide a big picture on the overall frictional behavior of material and be helpful in design and selection of material to meet the requirements for specific applications. For example, LFM has been used for studying of frictional and tribological properties of two-dimensional (2D) materials (e.g., graphene, MoS2, and h-BN) which are potential candidates as protective and solid lubrication coating layers for micro- and nano- devices [1,2]. However, LFM measurement is not always straightforward due to lack of guideline on experimental procedure and data interpretation. Especially, quantitative measurement of frictional properties can sometimes be cumbersome for a new AFM user. This study aims at providing a helpful approach on how to measure the quantitative frictional properties at the nano-scale using the AFM.

## How LFM works

The principle of LFM is similar to that of Contact mode AFM. In Contact mode, the vertical bending of cantilever is monitored while AFM tip scans on surface to collect information on surface morphology of the sample. In LFM, twist of the cantilever is additionally monitored to collect information on distribution of frictional properties across the sample surface. Fig. 1 presents schematic illustration of a typical LFM measurement. Essentially, the Z scanner will press the tip against the sample surface until a given vertical deflection setpoint, as denoted in Fig. 1(a). This setpoint force will be kept constant during scanning. To collect the LFM data, the tip should scan on the sample surface in a direction perpendicular to the cantilever axis (ΔX). The lateral (friction) force exerted at tip-sample interface will generate a torque τ that twists the cantilever about its axis, causing the displacement in lateral direction of the laser spot on the quadrant position sensitive photo detector (PSPD), as shown in forward scan and backward scan illustrations in Fig. 1(a). By monitoring the lateral signal while scanning forward and backward on the sample surface, a friction loop data can be generated, as shown in Fig. 1(b). The friction force acted between tip and sample is half width in vertical direction of the friction loop.

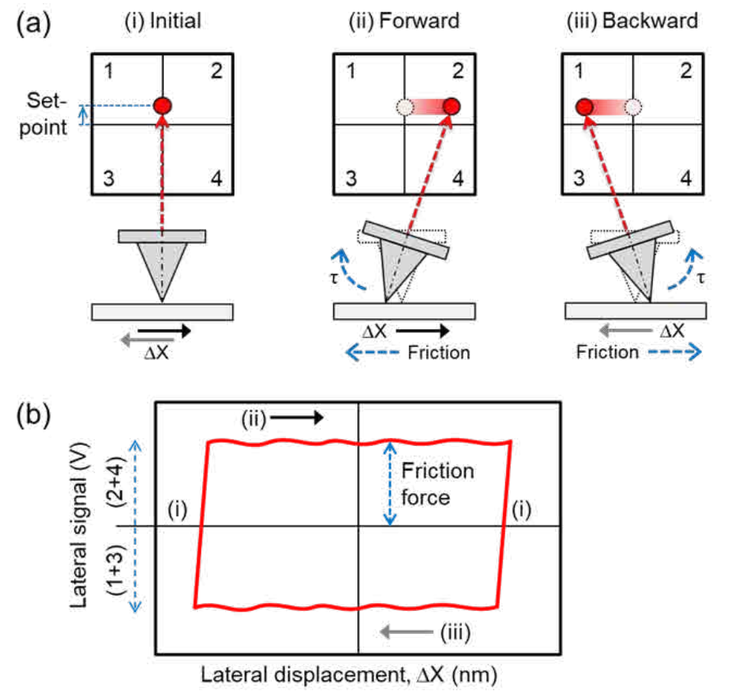


*Fig. 1. Illustration of a typical LFM measurement. In LFM, the laser spot displacement in vertical direction [(1 + 2) – (3 + 4)] and lateral direction [(2 + 4) – (1 + 3)] are monitored to provide information on surface topography and frictional properties of target sample. In (a), the cantilever behavior during scanning is shown. Friction-induced torque τ will twist the cantilever about its axis, leading to lateral displacement of the laser spot on PSPD. In (b), an example of friction loop obtained from LFM measurement is shown. The half width of lateral signal is defined as friction force in unit of volts.*

Example of LFM measurement

A Park NX10 AFM system was used in this study. To obtain a clear LFM signal, a cantilever with relatively low spring constant is preferred to enhance the lateral force sensitivity. In this regard, a conventional Si probe (PPP-CONTSCR, Nanosensors) with nominal spring constant of about 0.2 N/m was used for measurement. Prior to data collection, the cantilever was calibrated in both normal and lateral directions for quantitative normal and lateral force measurements, respectively. Fig. 2 presents a typical normal force calibration procedure in AFM. The normal deflection sensitivity or A – B sensitivity (in volts per micrometer) of the cantilever was determined by performing force-distance (FD) curve measurement on a rigid substrate (e.g., silicon or sapphire substrate). Generally, the A – B sensitivity can be calculated from linear portion of forward or backward curve using the integrated function of SmartScan AFM control software. However, as shown in the data Fig. 2(a), the A – B sensitivity determined from backward curve was found to be slightly larger than that of forward curve due to effect of sliding friction between the AFM tip and the sample in this work [3]. To eliminate this effect, the A – B sensitivity was calculated by taking average of values determined from forward and backward curves. As a result, A – B sensitivity was calculated to be 29.04 V/µm. Then, thermal noise method [4] was used to determine the normal spring constant of the cantilever. For a more representative result, about 200 thermal spectra were collected and averaged. The spring constant of the cantilever used was calculated to be 0.21 N/m, from the fitting result in Fig. 2(b).

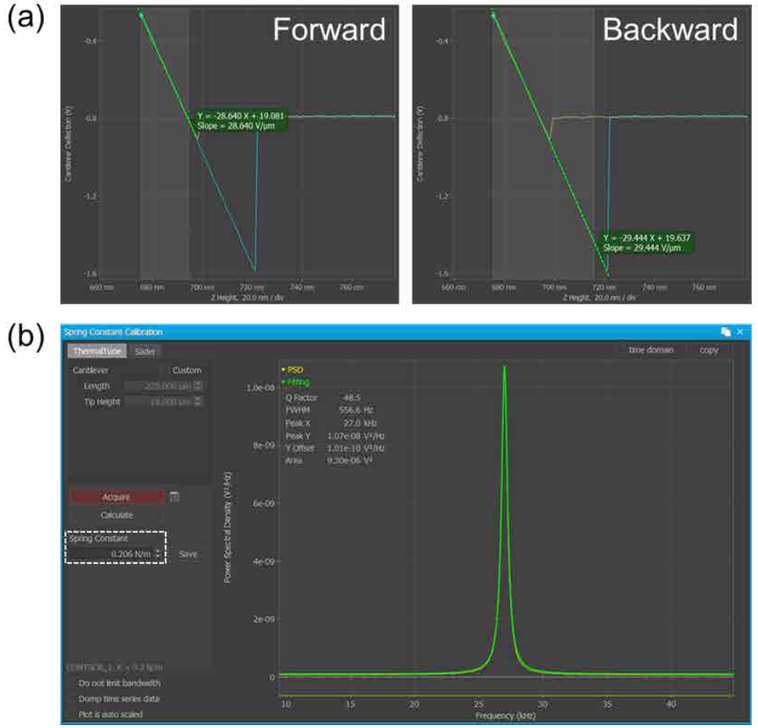


*Fig. 2. Example of normal force calibration in AFM. In (a) the A – B sensitivity of the cantilever was determined from the force-distance curve. In (b), the embedded thermal tune function can be used to calculate the spring constant of cantilever based on thermal noise method.*

Lateral AFM Thermal-Sader method [5–7] was used to determine the lateral force sensitivity of the cantilever. This method has advantages of simplicity, tip preservation, and good accuracy [5–7]. Thermal noise spectrum of the first torsional vibration mode of the cantilever was collected. A signal access module was used to connect LFM signal from the PSPD to A – B input of the controller, as shown in Fig. 3. Examples of normal and torsional vibration modes of the same cantilever are also presented in the figure. The first normal and torsional resonances were found to be at about 27 kHz and 278 kHz, respectively, for the cantilever used. Then, the first torsional mode of the cantilever was fitted to the simple harmonic

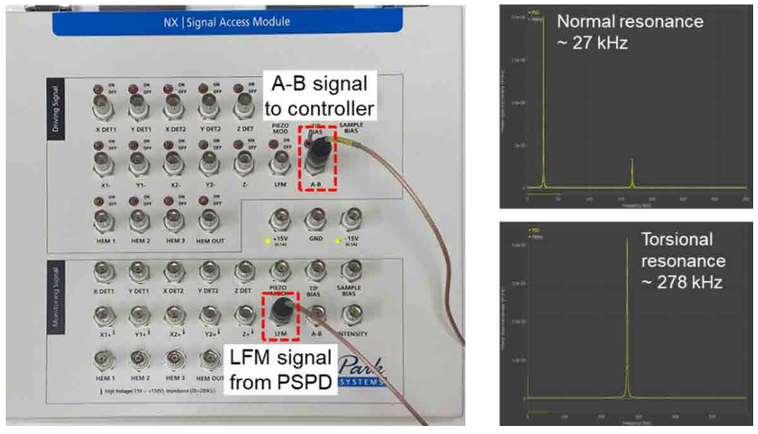


*Fig. 3. Experimental set-up for lateral calibration. The signal access module was used to direct the LFM signal from the PSPD to A – B input of the controller to collect the thermal noise spectrum of the first torsional vibration mode of the cantilever. Noted that the switch at A – B port can be turned off to collect normal thermal signal as usual and turned on to collect lateral thermal signal.*



oscillator (SHO) model to determine the dc power response P_dc, torsional resonance frequency f_T, and quality factor Q_T based on Eq. (1).

$$\mathrm{PSD(f)} = \mathrm{P_{white}} + \frac{\mathrm{P_{dc}} \times \mathrm{f_T^4}}{(\mathrm{f^2} - \mathrm{f_T^2})^2 + \frac{\mathrm{f^2} \times \mathrm{f_T^2}}{\mathrm{Q_T^2}}}$$

where PSD(f) is power spectral density as a function of frequency f, P_white is noise floor of thermal signal. Fig. 4 shows an example of the SHO model fit to the first torsional mode of the cantilever with P_white, P_dc, f_T, and Q_T as fit parameters. For lateral force sensitivity calculation based on Lateral AFM Thermal-Sader method, P_dc, f_T, and Q_T are required.

In the next step, torsional Sader method [8] was used to calculate the torsional spring constant k_T of the cantilever. For simplicity in calculation, an online calculator can be used [9]. The calculation requires length, width, torsional resonance frequency, and quality factor as inputs. The length and width of the cantilever can be determined using an optical microscope or from the nominal value provided by manufacturer. Finally, the lateral force sensitivity of the cantilever α (in volt per newton) was determined from Eq. (2) [7].

$$\alpha = \left(\mathrm{h} + \frac{\mathrm{t}}{2}\right)\sqrt{\frac{\pi \times \mathrm{f_T} \times \mathrm{P_{dc}} \times \mathrm{Q_T}}{2 \times \xi \times \mathrm{k_T} \times \mathrm{k_B} \times \mathrm{T}}}$$

where h is tip height, t is cantilever thickness, ξ is correction factor (assumed ξ =8/π^2 [7]), k_B is Boltzmann constant, T is absolute temperature. α value of the cantilever used in this study was calculated to be 0.012 V/nN.

After normal and lateral calibrations, the LFM measurement was performed on a thin flake of graphene deposited on a silicon (Si) substrate. The normal force (setpoint), scan area, and scan rate were set to 10 nN, 2**x**1 µm2, and 0.5 Hz, respectively. Relatively low scan rate was used to make sure that the tip could track the surface well. The topography and LFM channels were monitored during scanning.

LFM measurement result is summarized in Fig. 5. The height, lateral forward (FW), and lateral backward (BW) images along with the cross-sectional profiles are presented in the figure. The thickness of graphene layer estimated from the cross-sectional

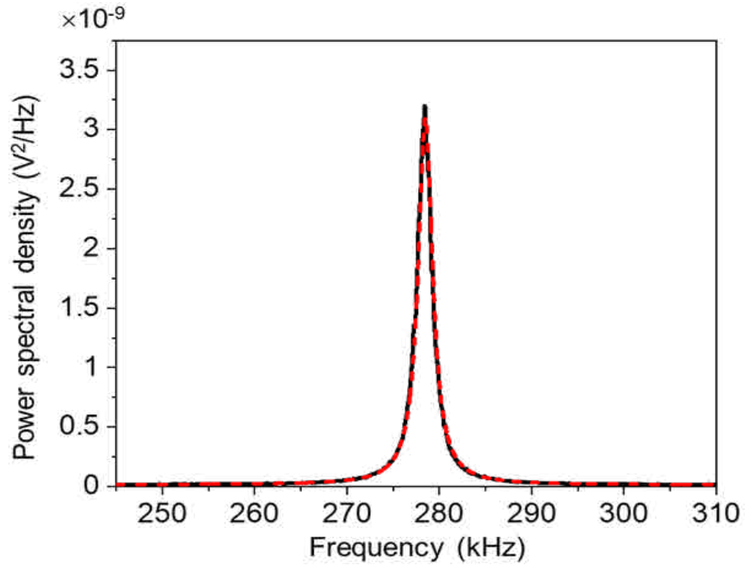


*Fig. 4. Thermal noise spectrum of the cantilever used. The red dashed line presents the curve fit based on simple harmonic oscillator model.*

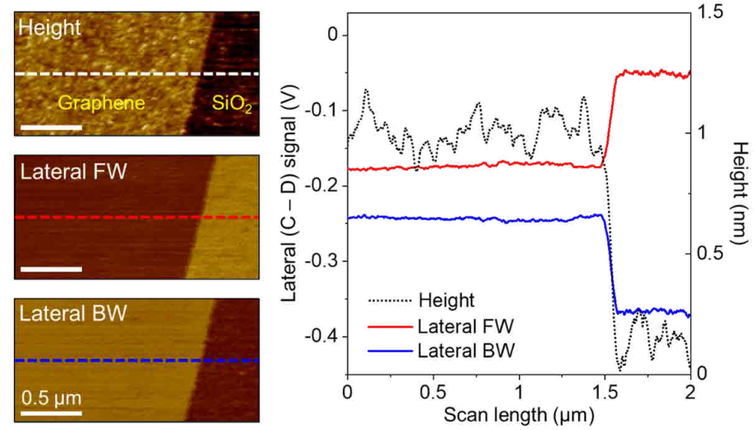


*Fig. 5. Height and lateral images obtained on a thin flake of graphene deposited on Si substrate. The lateral forward and backward signals at the same scan line form a friction loop that represents the friction characteristics of sample surface.*

height profile was about 1 nm. Also, the material effect on friction force is clearly shown in the friction loop data. It was clearly observed that Si substrate exhibits higher frictional properties compared to graphene sample. In addition, it should be noted that the lateral forward and backward signals are expected to be symmetrical about the zero-horizontal axis, as shown in Fig. 1(b). However, in practical measurement, the laser spot is not always located at the zero-lateral position [(2 + 4) = (1 + 3)] initially. As a result, the entire friction loop can be shifted upward or downward along the vertical axis. To eliminate the effect of this offset on calculation result, the friction force F_f can be calculated by considering both forward and backward scan directions, using Eq. (3). By subtracting the LFM backward signal from the LFM forward signal, the effect of vertical offset in friction loop on friction force calculation result is eliminated.

$$\mathrm{F_f} = \left(\frac{\text{LFM forward} - \text{LFM backward}}{2}\right) \times \alpha^{-1}$$

# Park Systems

## Dedicated to producing the most accurate and easiest to use AFMs

### General AFMs

Park Systems provides a range of popular AFMs for general research and industrial applications. Designed to be extremely versatile while still providing the accuracy and functionality necessary to do high quality work, our line of general AFMs offer researchers and engineers alike the ability to get extremely accurate results quickly and easily.

**Applications:**

- Materials Science
- Failure Analysis
- Semiconductor Analysis
- Hard Disk Media Analysis

### Park FX40

A Groundbreaking New Class of Atomic Force Microscope for Nanoscientific Research: The AutonomousAFM

### Park NX10

The premiere chioce for nanotechnology research

### Park XE7

The most affordable research grade AFM with flexible sample handling

### Park XE15

Power and versatility, brilliantly combined

### Park NX20

The premiere choice for failure analysis

### Park NX20 300 mm

The leading automated nanometrology tool for 300 mm wafer measurement and analysis



### Park NX-Hivac

The most advanced high vacuum AFM for failure analysis and sensitive materials research

### Park NX12

The most versatile AFM for analytical chemistry

### Industrial AFMs

Park Systems is dedicated not just to advancing research, but industry as well. That's why our designers have worked to build a line of the most effective AFMs for FA engineers and industrial applications.

**Applications:**

- Failure Analysis
- Semiconductor Analysis
- Hard Disk Media Analysis

### Park NX-Hybrid WLI

The AFM and WLI technologies built into one seamless system

### Park NX-TSH

The automated Atomic Force Microscopy (AFM) system for ultra large and heavy flat panel displays at nanoscale

### Park NX-3DM

Automated industrial AFM for high-resolution 3D metrology

### Park NX-Wafer

Low noise, high throughput atomic force profiler with automatic defect review

### Park NX-PTR

Fully automated AFM for accurate inline metrology of hard disk head sliders

### Park NX-HDM

Simply the best AFM for media & substrate manufacturing

Fig. 6 shows the friction force calculation result based on Eq. (3). Friction force was determined to be 2.9 nN and 13.7 nN when the tip slide against graphene and Si substrate, respectively. The friction force obtained on Si increases by a factor of 4.7 compared to the graphene flake. Low friction characteristics of graphene suggests it can be a potential candidate as solid lubrication layer for moving mechanical parts of micro- and nano- devices.

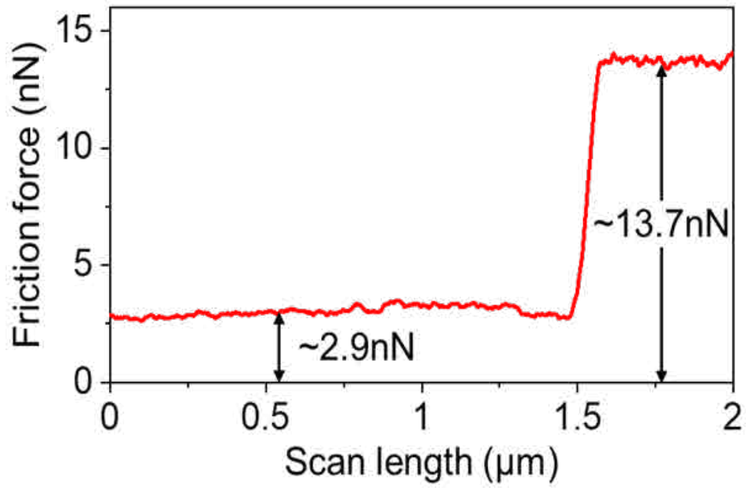


*Fig. 6. Friction force calculated from the friction loop in Fig. 5. The silicon substrate exhibits higher frictional properties than the graphene sample.*

**Conclusions**

This work presents an example on how to utilize the AFM as a properties characterization tool at the nano-scale. In particular, step-by-step procedures on how to collect and to interpret the friction data are also discussed. The outcome is expected to provide a helpful guideline for quantitative frictional properties measurement using AFM.

Nevertheless, there are a few criteria should be met for more accurate frictional properties measurement. In-plane spring constant of the cantilever should be large enough so that only twist of the cantilever occurs during lateral scanning [10]. To improve the accuracy of lateral force sensitivity determination based on Lateral AFM Thermal-Sader method, the cantilever geometry should meet the criterion of Sader's method (i.e., high length-to-width ratio) [5,7]. Also, the torsional resonance of the cantilever should not exceed the bandwidth of the AFM instrument. Usually, conventional cantilevers for LFM measurement satisfy these criteria. However, for special cases (e.g., home-made cantilever, modified cantilever), it is recommended to check these criteria before measurement.

**References**


[1] D. Berman, A. Erdemir, A. V Sumant, Graphene: a new emerging lubricant, Mater. Today. 17 (2014) 31–42.
[2] B.-C. Tran-Khac, H.-J. Kim, F.W. DelRio, K.-H. Chung, Operational and environmental conditions regulate the frictional behavior of two-dimensional materials, Appl. Surf. Sci. 483 (2019) 34–44.
[3] Q.D. Nguyen, K.-H. Chung, Effect of tip shape on nanomechanical properties measurements using AFM, Ultramicroscopy. 202 (2019) 1–9.
[4] J.L. Hutter, J. Bechhoefer, Calibration of atomic-force microscope tips, Rev. Sci. Instrum. 64 (1993) 1868–1873.
[5] K. Wagner, P. Cheng, D. Vezenov, Noncontact Method for Calibration of Lateral Forces in Scanning Force Microscopy, Langmuir. 27 (2011) 4635–4644.
[6] N. Mullin, J.K. Hobbs, A non-contact, thermal noise based method for the calibration of lateral deflection sensitivity in atomic force microscopy, Rev. Sci. Instrum. 85 (2014) 113703.
[7] B.C. Tran Khac, K.-H. Chung, Quantitative assessment of contact and non-contact lateral force calibration methods for atomic force microscopy, Ultramicroscopy. 161 (2016) 41–50.
[8] C.P. Green, H. Lioe, J.P. Cleveland, R. Proksch, P. Mulvaney, J.E. Sader, Normal and torsional spring constants of atomic force microscope cantilevers, Rev. Sci. Instrum. 75 (2004) 1988–1996.
[9] Online calculator is available at: http://www.ampc.ms.unimelb.edu.au/afm/calibration.html.
[10] J.E. Sader, C.P. Green, In-plane deformation of cantilever plates with applications to lateral force microscopy, Rev. Sci. Instrum. 75 (2004) 878–883.




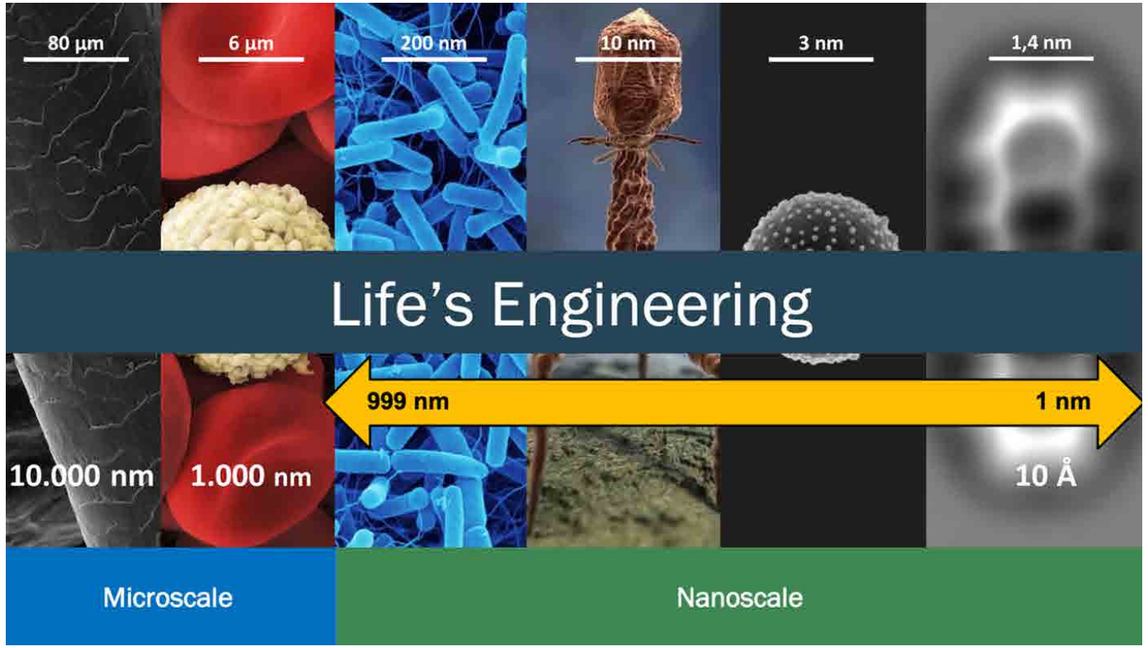


*"Nanotechnology is Life's Engineering, and has been present in our lives since its beginning, closely linked to the functioning of organisms and an essential part of Nature's tools to create all its diversity"*

*Image created by Leandro Antunes Berti*

## President, Dr. Leandro Berti

*President of BrasilNano – The Brazilian Nanotechnology Association and CEO of FIBER INOVA – a strategic innovation consultancy company.*

Leandro Berti has over 20 years of experience in Nanotechnology and Advanced Technologies and current is the CEO of FIBER INOVA (www.leandroberti.com.br) and President of BrazilNano – The Brazilian Nanotechnology Association. Berti studied Computer Engineering at the University of Itajai Valey (UNIVALI), earned his PhD in Nanotechnology at the University of Sheffield (UK) and his Post-doctorate in Nanobiotechnology at the Federal University of Santa Catarina (UFSC – BR).

Creator and Coordinator of the SUPERHUB of Nanotechnology of Paraná, Manager of Graphene Projects in the Automotive Industry at SAE Brazil. He served as Head of Key Enabling Technologies and Head of Strategic Technologies at the Ministry of Science, Technology, Innovation in Brazil (MCTI), responsible for national public policy, strategy for Nanotechnology, Photonics, Advanced Materials and Industry 4.0. Created the National Action Plan for Key Enabling Technologies; Included Nanotechnology in the Route 2030 program, created the Legal Framework for Nanotechnology and Advanced Materials. He served as a member of the Science and Technology Committee of the National Council of Science and Technology, BRICS WG Photonics National Representative, OECD BNCT - Nanotechnology National Representative, Brazil-Canada Joint Committee for Cooperation on Science, Technology and Innovation; Director of the Brazilian-Argentine Center for Nanotechnology, President of the Brazilian-Chinese Center for Nanotechnology. He also served as the Executive Secretary of API. nano at CERTI Foundation. Author of the first book on regulation with Nano safety in Brazil.

As the Head of Key Enabling Technology at the Ministry of Science and Technology in Brazil and under his leadership released the first National Action Plans for Key

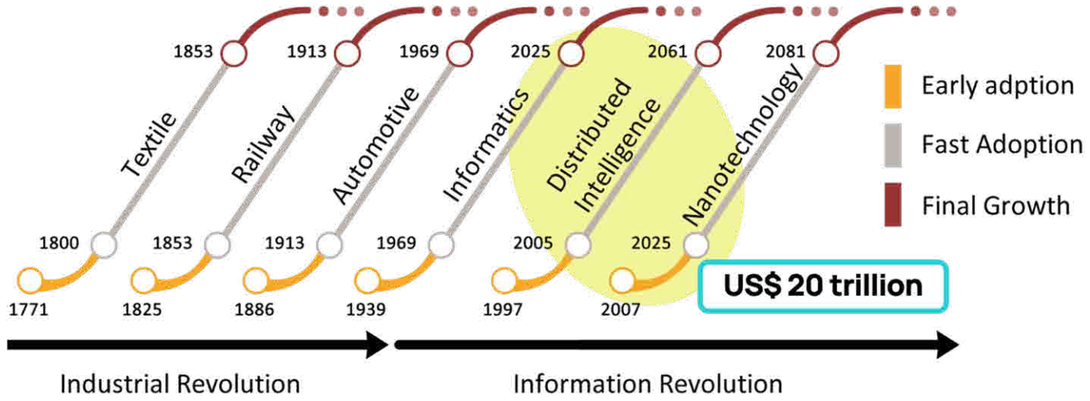


*Image created by Leandro Antunes Berti (refences from LuxResarch, product.statnano.com, http://www.oecd.org/sti/nanotechnology-indicators.htm).*

Enabling Technologies , currently in use, whose main focus is to promote integration between academia and industry by means of Technology-push and Demand-pull. On the Technological-push side are the National Systems and Programs, the Public and Private Laboratories, the Research Technology and Innovation Organizations (RTOs) and the Higher Education aligned with the Action Fronts in Nanotechnology, Photonics, Advanced Materials and Technologies for Industry 4.0 (4IR). On the other side is the Demand-pull that connects with the action fronts through attraction elements, which are concrete actions for the construction of consistent and robust bridges for science and technology to reach the market through innovation. He also pioneered the inclusion of Society 5.0 as one of the main policies for the success of Industry 4.0 in Brazil.

The main form of molecular assembly at the nanoscale is self-assembly, a natural process where separate or linked components spontaneously form larger structures. The material that makes up cell structures, such as proteins, enzymes and even DNA itself, are nano in size. Understanding and applying this vision that values the natural has always benefited humanity. The new properties of nanomaterials discovered from the understanding nature, revolutionize not only products, but also capital goods – production machines – and the provision of services, with innovations that until now were unimaginable.

According to the Kondratiev cycle, the new wave of economic growth is Nanotechnology, and in recent years (2020) has reached US$ 20 trillion, mainly to the immense increase of products to fight the coronavirus pandemic. An example, is the graphene market, which has an estimated value of US$ 100 to 20 thousand for each kilogram of material, could reach US$ 876 million in 2027 with a CAGR of 41% (2020 – 2027), with applications in electric batteries, tires, conductive paints, flexible electronics, smart concrete, among others. The pervasive nature of Nanotechnology allows it to reach even larger markets such as the Internet of Things (IoT). The IoT international road mapping report, from the Smart Action – Innovating beyond IoT , presents a series of advantages and improvements that Nanotechnology adds to IoT solutions. The report also emphasizes that the priority themes are energy storage and generation, nanoelectronics, nanosensors, nanomaterials and even nanomachines, nanonetworks and the Internet of Nanothings (IoNT). IoT is one of the tools of Industry 4.0 that allows the integration of new nanosensors connected in a network to, for example, control the forecast of production and losses in real time, a market worth billions of dollars.

The industry 4.0, has several names and representations, in the European Community it is known as Industrial Renaissance (Industrial Renaissance), in Germany as Industry 4.0, in the US as Advanced Manufacturing, but in fact they seek the growth and post-crisis modernization of the globalized world. It is characterized by the integration and remote control of production, from sensors, equipment and machines connected in a network (automation and systems digitization associated with cyber physical systems). Is a philosophy, a cultural change in essence, it is not only related to the production of electronics, but also to Intelligent Production, and with important application in the traditional sector of agriculture, health and goes far beyond what is recommended in several reports, as its greatest impact will be on world geopolitics.

The Digital Transformation (DX) is a means to achieve the industry 4.0. Digital Transformation without Nanotechnology and other strategic technologies is not feasible. Just relying on IT to implement the Digital Transformation is a simplification and might lead us to unsustainable path. It's important to understand that the path to Industry 4.0 is in the convergence of many technologies that are complementary to each other. However, we need to solve this puzzle placing and connecting the outputs of those technologies to create the best possible path to achieve Industry 4.0. As an example of applying the concept of Industry 4.0 in agriculture, is the integration of various nanosensors and IoT equipment to monitor the soil, the climate, the position of the soy pod or apple tree, to ensure the production of the best grain from soy or the best apple that local conditions allow. All this connected in a network, with production and losses forecast in real time, called Agriculture 4.0. In healthcare, an application example is the remote control of medical equipment that will facilitate the monitoring of patients, reducing the response time for emergencies. We recently saw a soaring increase of technologies derived from mRNA, in special the new corona virus vaccine technology. In fact, this new form of delivering the agent to fight the disease is way beyond vaccines, it's a comprehensive platform to create a better vehicle to delivery drugs to the right target. That has open up a new era for pharmaceutical companies, called Health 4.0.

Another important fact that is beyond IoT, is that Industry 4.0 requires machinery that is resilient, durable and robust enough to be able to complete the new worldwide production journey, which will be high volume, high frequency, high speed, highly customized and unsupervised. One of the main candidates to enable Industry 4.0 is Graphene, a 2D material type, with two-dimensional layers, which has fantastic properties, such as: ballistic conductivity (100x Copper), accelerated cooling (500 W/mK), mechanical strength (100x Steel), ultraflexible (< 200 MPa ) and impervious to fluids (omniphobic). Therefore, the machinery must support production cycles much longer, faster and more demanding than those currently practiced, and Graphene is here to help.

If we look closely, every time the humanity discovers a new phenomenon, we are enticed to create new technology. For example, when we discover fire, the human took ages to control it and benefit from it, in a Hunting Society. Many more years and we develop irrigation techniques and start establishing settlements, but even in that Agrarian Society we had no idea on how to use the fire, unless for cooking raw food. Humans had evolved very slowly until they starting trading goods across the globe, and with the advent of Coffee Shops (1652), the population that mostly drank fermented beverages and stayed in a light drunk state, are now drinking a reinvigorating beverage such as coffee and tea. That made us more awake and new ideas started to flow, and one the ideas that flourished the most was the Steam Machine, a machine powered by fire that produced steam. Now the humans could create the beginnings of automation, and gave rise to the Industrial (Revolution) Society. From that point onwards we have seen an enormous amount of technology been created and society evolve a thousand times faster than before.

The lesson here is that society had to evolve beyond the control of fire to be able

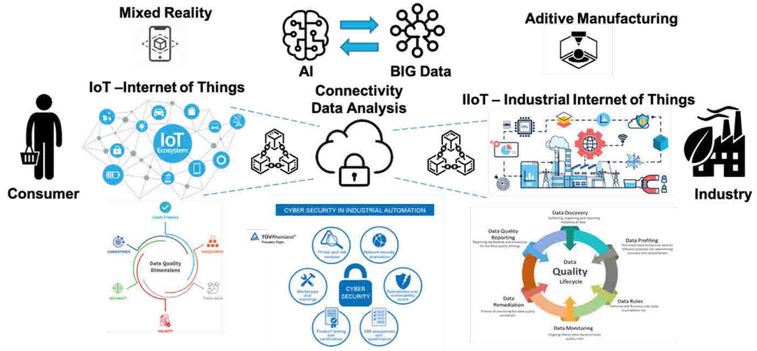


*Digital Transformation (DX), image created by Leandro Antunes Berti.*

to fully benefit from it.
That has been always true and for us to fully benefit from Industry 4.0 we need be in the Society 5.0.

***"For society to fully benefit from Industry 4.0 we need be in the Society 5.0"***

The Japanese government together with the Federation of Industries of Japan (Keidanren) identified that society will advance towards becoming a super-intelligent society (Society 5.0) , demonstrating an environment increasingly connected with harmonious coexistence with robots and autonomous machines, the seamlessly integration of the physical world and the digital world – phygital (physical-digital). This social change is need to address the issues of increasing population age, low birth rates, limited electricity, natural disasters, security and social inequality. The Society 5.0 concept goes further and has the main objective of converging all existing technologies to improve the quality of life in general. The advent and access to new technologies allow the emergence of new production chains, better adapted to national and global reality. Unveiling this advanced society with an elderly majority requires not only the re-qualification of experienced labor (healthy aging), but also a more qualified workforce. Workers versed in the most diverse technological advances, more productive, and who know how to live with sudden changes, increasingly present in everyday life. Failure to meet this need can cause a destabilization of social security, leading to the loss of at least a generation of workers. Key components of today's society such as health, recreation, work, consumption, mobility, education and security will be profoundly impacted. This new society that is the result of the revolution in Technologies for Advanced Manufacturing will be more demanding, as the customization of products and services will reach a very high level. However, to obtain products and services that aim to increase the quality of life, reduce social inequalities and increase awareness of environmental preservation, technological solutions must overcome five obstacles: 1) State Bureaucracy Wall: formulation of national strategies, through real integration and effective dialogue between ministries and government agencies; 2) The legal system Wall: reduction of interventionism and approval of laws that facilitate and encourage innovation; 3) Technology Wal: promote technologies related to cyber security, Artificial Intelligence and robotics; and the guarantee of a minimum budget for R&D+I and technological development; 4) Human resources Wall: promote an educational reform that promotes the teaching of information technologies and emerging technologies, that encourages creativity and creates highly skilled professionals); and 5) Social acceptance Wall: building a "social consensus" through dialogue with society that discusses everything from the relationships between people and machines to the meanings of "happiness" and "personal satisfaction". Conquering these obstacles will enable society to overcome not only the challenges of innovation and technological advancement, but also to achieve UN's Sustainable Development Goals (SDGs). In particular, in the social aspect, Graphene meets at least 11 of the 17 SDGs and its versatility and breadth of

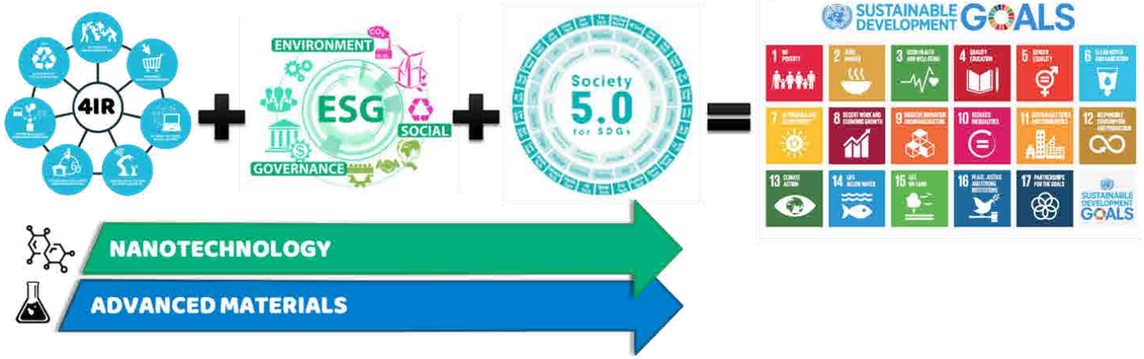


*Image created by Leandro Antunes Berti*

applications allows Graphene to be one of the main materials for a sustainable future . This leads us to understand that Graphene is an integral part of the generation of a new society centered on the generation of value, sustainable in the four axes: political, social, economic and environmental, is phygital and strengthens the ESG adoption. That is the Nexus between Nanotechnology and Society 5.0.

**References**

[1]KET - Brazilian National Plan https://antigo.mctic.gov.br/mctic/opencms/salaImprensa/noticias/arquivos/2018/10/MCTIC_lanca_plano_de_acao_para_o_desenvolvimento_da_nanotecnologia_e_da_industria_40_no_Brasil.html
[2]IoT International Roadmapping, Smart Action (http://cordis.europa.eu/docs/projects/cnect/4/609024/080/deliverables/001-20150630udesmartactionIoTInternationalRoadmapd22puAres20152863783.pdf)
[3]Keidanren – Federação das Indústrias do Japão, (http://www.keidanren.or.jp)
[4]Graphene Flagship – https://graphene-flagship.eu/graphene/news/graphene-is-sustainability/





# EVALUATION OF LOCAL MECHANICAL AND CHEMICAL PROPERTIES VIA AFM AS A TOOL FOR UNDERSTANDING THE FORMATION MECHANISM OF PULSED UV LASER-NANOINDUCED PATTERNS ON AZO-NAPHTHALENE-BASED POLYIMIDE FILMS

**Iuliana Stoica 1*, Elena-Luiza Epure 2, Catalin-Paul Constantin 1, Mariana-Dana Damaceanu 1, Elena-Laura Ursu 1, Ilarion Mihaila 3 and Ion Sava 1**

*"Petru Poni" Institute of Macromolecular Chemistry, 700487 Iasi, Romania; constantin.catalin@icmpp.ro (C.-P.C.); damaceanu@icmpp.ro (M.-D.D.); ursu.laura@icmpp.ro (E.-L.U.)*
*Faculty of Chemical Engineering and Environmental Protection, "Gheorghe Asachi" Technical University, 700050 Iasi, Romania; lepure@tuiasi.ro*
*Integrated Center of Environmental Science Studies in the North-Eastern Development Region (CERNESIM), "Alexandru Ioan Cuza" University of Iasi, 700506 Iasi, Romania; ilarion.mihaila@gmail.com*
** Correspondence: stoica_iuliana@icmpp.ro (I.S.); isava@icmpp.ro (I.S.)*

**Abstract:** Aromatic polyimides containing side azo-naphthalene groups have been investigated regarding their capacity of generating surface relief gratings (SRGs) under pulsed UV laser irradiation through phase masks, using different fluencies and pulse numbers. The process of the material photo- fluidization and the supramolecular re-organization of the surface were investigated using atomic force microscopy (AFM). At first, an AFM nanoscale topographical analysis of the induced SRGs was performed in terms of morphology and tridimensional amplitude, spatial, hybrid, and functional parameters. Afterward, a nanomechanical characterization of SRGs using an advanced method, namely, AFM PinPoint mode, was performed, where the quantitative nanomechanical properties (i.e., modulus, adhesion, deformation) of the nanostructured azo-polyimide surfaces were acquired with a highly correlated topographic registration. This method proved to be very effective in understanding the formation mechanism of the surface modulations during pulsed UV laser irradiation. Additionally, to AFM investigations, confocal Raman measurements and molecular simulations were performed to provide information about structured azo-polyimide chemical composition and macromolecular conformation induced by laser irradiation.

## Introduction

Polyimides (PIs) represent an important class of high-performance polymers that are exploited in a variety of applications due to their excellent physicochemical properties such as optical and thermal stability in combination with high glass transition temperature, low susceptibility to laser damage, and low dielectric constant value [1,2]. Moreover, polyimides have been investigated as potential materials in the fields of optoelectronics and photonics [3]. Particularly interesting are polyimides containing azobenzene units, which have already been investigated for photoinduced alignment in liquid crystal dis- play [4], as photomechanical response materials [5], and for holographic diffraction grating recording [6–11].

This study focuses on the investigation of a newly synthesized aromatic polyimide containing azo-naphthalene side groups with the aim to evaluate the local morphological, mechanical, and chemical properties via atomic force microscopy, especially in PinPoint mode, and confocal Raman spectroscopy. It is meant to provide a deep understanding of the formation mechanism of SRGs induced by pulsed UV laser on these azopolyimide films, through phase masks, using different fluencies and number of pulses. Moreover, this article attempts to correlate the macroscale behavior of this azo-naphthalene-based polyimide during photoisomerization with the one from the atomic level simulating certain polymeric systems with a different content of the cis isomer.

## Materials, Methods and Measurements

An aromatic diamine containing the azo group (-N=N-) pendent to the triphenyl-methane core was synthesized by the Williamson reaction of 4-[bis-(4-amino-3-methyl- phenyl)-methyl]-phenol with 3-[4-naphthalen-1-ylazo)-phenoxy]-bromopropane. The azopolyimide has been synthesized by the polycondensation reaction of 6FDA with the above mentioned azodiamine. The structure of the azo- naphthalene-based polyimide is shown in Figure 1. The thickness of the azo-naphthalene- based polyimide films, measured using a profilometer, was 3094–3117 nm, the average value being 3.10 ± 0.01 µm.

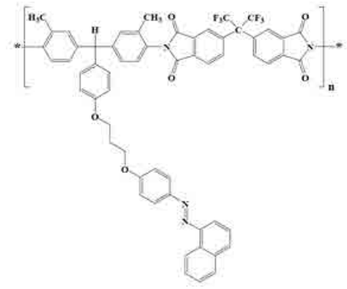

*Figure 1. Chemical structure of the novel azo-naphthalene-based polyimide, AzoPI, used in this study.*

In order to induce micro/nano structuration on the azo-polyimide surface, the setting presented in Figure 2 was used.

Nanomechanical measurements were made on a Park NX10 Atomic Force Microscope (Park Systems Corp., Suwon, Korea), using PinPoint Nanomechanical mode, which allowed us to obtain sample's stiffness mapping through force–distance curves acquired at each pixel over the entire scanning area (of 1 × 5 µm2 in our case). Thus, the quantitative nanomechanical properties (i.e., modulus, adhesion, deformation) of the nanostructured azo-polyimide surfaces were acquired with highly correlated topographic registration. In order to provide the most accurate mechanical properties data, we carefully selected the Force Modulation Mode - Reflex Coating (FMR) probe (Park Systems Corp., Suwon, Korea) with a force constant of 2.8 N/m and resonance frequency of 75 kHz

according to the relative stiffness of their cantilever when compared to that of the sample, so that it can offer immediate response to any changes on the surface's material properties. The scanning frequency was 0.5 Hz, and the scanning speed was 5.0 µm/s.

## Results and Discussion

### *Nanomechanical Characterization Using AFM PinPoint Mode*

PinPoint Nanomechanical mode was designed to prevent positional errors by simultaneously acquiring accurate height and force–distance information in each of the 256 × 256 pixels in the whole scanning area, thus preventing the occurrence of the artifacts and positional errors in force–distance spectroscopy and topographical data. In Figure 5 and Appendix B, we present the working mechanism of PinPoint Nanomechanical mode, describing the generation of the map of the sample's stiffness/elasticity and deformation depth from the surface concomitantly obtained through the adhesion force map with the topographic sample information [59–64].

Figures 6–8 show the PinPoint combined height, adhesion force, deformation, and Young's modulus AFM images and corresponding cross-section profiles in the case of pristine (Figure 6) and irradiated azo-polyimide with a laser energy density of 45 mJ/cm2 and either 10 pulses (Figure 7) or 100 pulses (Figure 8). The last two samples were selected for this kind of measurement because the generated modulations were very well defined, facilitating the investigations in different positions of interest (on the top hills, middle slopes, base, and bottom valleys of the SRG, as indicated in Figure 5).

## Conclusions

The aim of this study was to provide new insights regarding the formation mechanism of pulsed UV laser-nano induced patterns on azo-naphthalene-based polyimide films by evaluating the morphological, statistical, local mechanical, and chemical properties via AFM, in correlation with the molecular modeling. The quantitative nanomechanical properties (Young's modulus, adhesion, deformation) of SRGs using the AFM PinPoint method were acquired with highly correlated topographic registration. The experimental evaluations highlighted different values of nanomechanical parameters obtained in

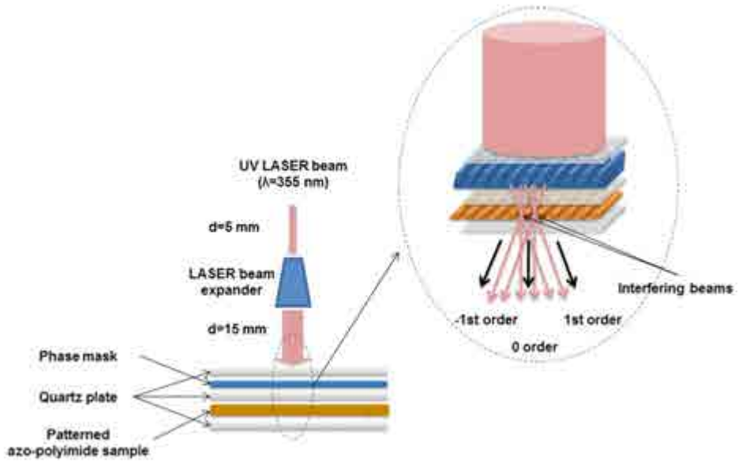


*Figure 2. Pulsed laser irradiation through a phase mask setting, with a detail on the formation of interference image on the azo-naphthalene-based polyimide surface.*

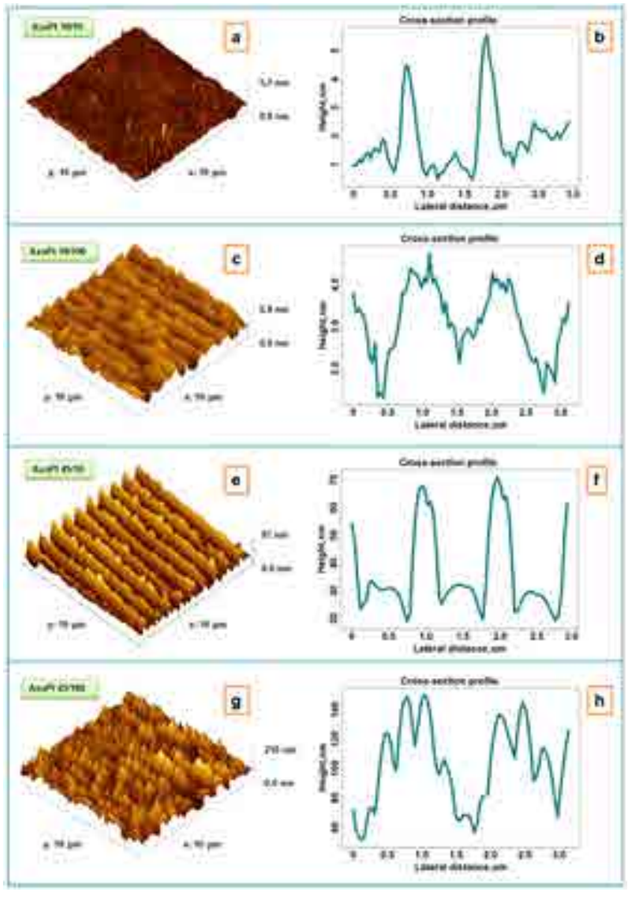


*Figure 3. Height 3D atomic force microscopy (AFM) images and corresponding cross-section profiles for azo-polyimide irradiated using different laser energy density/number of pulses of irradiation: 10 mJ/cm2 /10 pulses (a,b), 10 mJ/cm2 /100 pulses (c,d), 45 mJ/cm2 /10 pulses (e,f), 45 mJ/cm2 /100 pulses (g,h).*

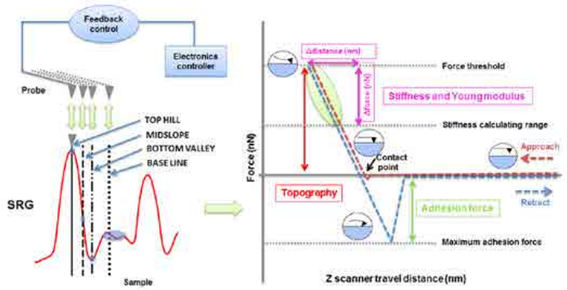


*Figure 5. Working mechanism of PinPoint Nanomechanical mode: the tip of the cantilever is moved at each of 256 × 256 points along a sample's surface, and the feedback system controls the approach and retraction of a probe, allowing the acquirer of both surface topography and force–distance curves, and further to extract the mechanical property data.*

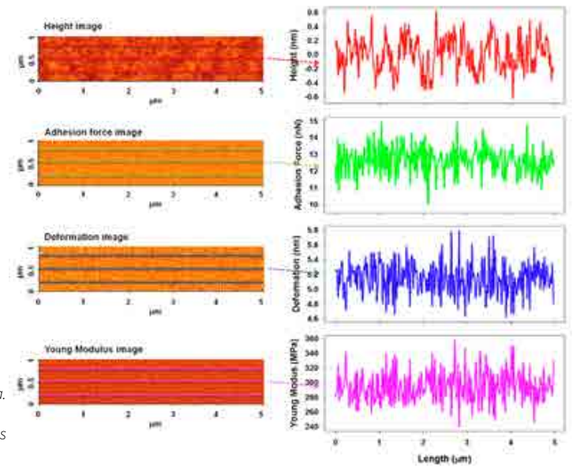


*Figure 6. AFM PinPoint combined height, adhesion force, deformation, and Young's modulus images and representative cross-section profiles taken along the middle line obtained for pristine azo-polyimide.*




*Figure 7. AFM PinPoint combined height, adhesion force, deformation, and Young's modulus AFM images and corresponding cross-section profiles mediated from the presented three lines obtained for azo-polyimide irradiated with a laser energy density of 45 mJ/cm2 and 10 pulses. Figure 8. AFM PinPoint combined height, adhesion force, deformation, and Young's modulus images and corresponding cross-section profiles mediated from the presented three lines obtained for azo-polyimide irradiated with a laser energy density of 45 mJ/cm2 and 100 pulses.*

different regions of the patterned relief. These were induced by re-organization of the matter by azo-naphthalene dipoles orientation and material photo-fluidization induced by repeated trans–cis isomerization of the azo-segments. Attempts have been made to explain experimental phenomena by molecular modeling. The photoisomerization phenomenon was studied using three systems in which the content of cis isomers was gradually increased. Although the variations of the statistical and dynamic parameters such as the fractional free volume, end to end distance, mean square displacement, or dipole moment were small from one system to another, their evolution followed the same behavior as that observed at the macroscale during the photo-isomerization process. It was found that polymers with 50% azo groups in cis had either a maximum or a minimum peak of the calculated parameters. The low mobility of the chains with a maximum content in the cis isomer could explain the phenomenon of azopolymer hardening due to the photoisomerization process.

In addition, confocal Raman measurements evidenced no significant spectral changes, except for the slight increase of the absorption band due to the cis isomer evolution, demonstrating their origin in the polymer conformations before and after irradiation rather than in the polyimide chemical modifications.

To download the complete original article, please go to https://bit.ly/3oQLtZ0
This article originally appeared on Nanomaterials 2021, and condensed by NanoScientific under Creative Commons Attribution License

# SIMULTANEOUS ACQUISITION OF CURRENT AND LATERAL FORCE SIGNALS DURING AFM FOR CHARACTERISING THE PIEZOELECTRIC AND TRIBOELECTRIC EFFECTS OF ZNO NANOROD

Yijun Yang, Kwanlae Kim Department of Manufacturing Systems and Design Engineering (MSDE), Seoul National University of Science and Technology (SeoulTech), Seoul, 01811, Republic of Korea Scientific Reports volume 11, Article number: 2904 (2021) https://www.nature.com/articles/s41598-021-82506-8

**Abstract**

Atomic force microscopy (AFM) is central to investigating the piezoelectric potentials of one-dimensional nanomaterials. The AFM probe is used to deflect individual piezoelectric nanorods and to measure the resultant current. However, the torsion data of AFM probes have not been exploited to elucidate the relationship between the applied mechanical force and resultant current. In this study, the effect of the size of ZnO nanorods on the efficiency of conversion of the applied mechanical force into current was investigated by simultaneously acquiring the conductive AFM and lateral force microscopy signals. The conversion efficiency was calculated based on linear regression analysis of the scatter plot of the data. This method is suitable for determining the conversion efficiencies of all types of freestanding piezoelectric nanomaterials grown under different conditions. A pixel-wise comparison of the current and lateral force images elucidated the mechanism of current generation from dense arrays of ZnO nanorods. The current signals generated from the ZnO nanorods by the AFM probe originated from the piezoelectric and triboelectric effects. The current signals contributed by the triboelectric effect were alleviated by using an AFM probe with a smaller spring constant and reducing the normal force.

## Introduction

The piezoelectric effect of ZnO nanorods was first reported by Wang and Song in 20061. Subsequently, an atomic force microscopy (AFM) tip was used to deflect vertically grown ZnO nanorods at the submicron scale. Because ZnO exhibits semiconducting and piezoelectric properties, the strain induced in the individual ZnO nanorods by the AFM tip drives a flow of electric charge carriers through the metal-coated AFM tip and ZnO nanorods. Furthermore, the correlation between the topography signal and conductive atomic force microscopy (C-AFM) signal was analyzed to elucidate the underlying mechanism responsible for the generation of a piezoelectric potential in ZnO nanorods and to detect the current signal via the AFM tip. Through this experimental study, it was shown that the current signal during C-AFM is detected when the AFM tip touches the compressed side of an n-type ZnO nanorod9, as presented in Fig. 1. This comparative analysis of the topography and C-AFM signals also helped elucidate the piezoelectric effect in p-type ZnO nanorods and improved understanding of the effects of the ZnO nanorod growth method used on the piezoelectric power generation characteristics of the resulting nanorods. C-AFM is used preferentially to investigate the piezoelectricity of one-dimensional nanomaterials with wurtzite structures, such as CdS, CdSe, ZnS, InN, and GaN.

**Figure 1**

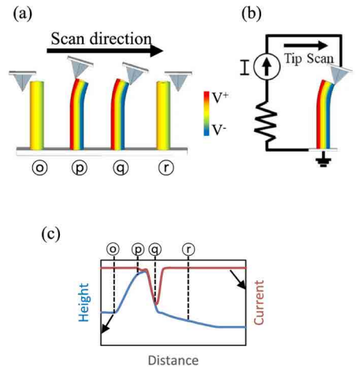


Piezoelectric potential induced by the AFM probe. (a) Generation of piezoelectric potential by deflection of the ZnO nanorod, (b) current passing through the metal-coated AFM tip in contact with the ZnO nanorod, (c) topography and C-AFM signals during the process in (a). The current signals originating from the piezoelectric potential are detected when the AFM tip touches the compressed side of an n-type ZnO nanorod.

Various types of sensors and energy harvesters based on piezoelectric nanomaterials and with a range of structures have been investigated. As these nanomaterials are often subjected to external mechanical forces, understanding their mechanical properties is important. Considering the size of these nanomaterials, lateral force microscopy (LFM) is an effective tool for investigating the elastic moduli of nanomaterials such as ZnO, Au, Si, and W nanowires. To perform mechanical tests accurately on a single nanowire, AFM scanning is conducted along a programmed manipulation path to deflect the nanowire. However, AFM scanning in contact mode also results in the deflection of vertically grown nanorods.

Typically, LFM involves measuring the degree of torsion induced in the AFM cantilever by the surface friction using a position-sensitive photodetector (PSPD). However, when studying the mechanical properties of nanorods, the lateral force applied to the AFM tip may be regarded as the lateral force to which the nanorods are subjected by the AFM tip. Accordingly, by simultaneously monitoring the C-AFM and LFM signals obtained while imaging vertically grown piezoelectric nanorods, the ratio of the output current to the lateral force applied to the ZnO nanorods can be determined. We observed the variations in the C-AFM current signal in response to the application of a lateral force to ZnO nanorods by simultaneously performing C-AFM and LFM. The degree of torsion of an AFM probe can be monitored during AFM operation (including C-AFM) by integrating the AFM instrument with a scanning electron microscope. In particular, Wen suggested that the triboelectric effect and contact potential as well as the piezoelectric effect are responsible for the current signals detected from ZnO nanorods using an AFM probe. However, this method requires a sophisticated experimental arrangement.



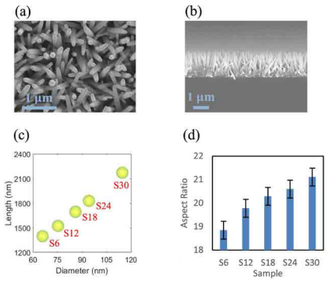


*Figure 2*

Conversely, the C-AFM and LFM signals can be readily acquired simultaneously during AFM operation in contact mode. In this work, this novel experimental method was used to study the effect of the ZnO nanorod size on the efficiency of conversion of the mechanical force to which they are subjected into current via the piezoelectric and triboelectric effects. Note that if five ZnO nanorod samples with distinct sizes are deflected by the same AFM tip with a constant normal force, the variation in the lateral force would approximately represent the variation in the net applied mechanical force. Thus, five ZnO nanorod samples with distinct aspect ratios were prepared, and the ratio of the output current to the mechanical force applied to the nanorods was determined. With respect to AFM-based studies of the piezoelectric effect of ZnO nanorods, the choice of the AFM probe may have a determining effect on the results, because the normal force in contact mode is determined by the spring constant of the AFM probe. Therefore, the ratio of the output current to the lateral force was determined using two AFM probes with different spring constants. Finally, we attempted to elucidate the mechanism responsible for the generation of current signals in ZnO nanorods by the AFM tip based on a scatter plot of the current signal versus lateral force and pixel-wise comparison of the C-AFM and LFM images. We confirmed that the piezoelectric and triboelectric effects mainly contribute to the current signals from ZnO nanorods detected by the AFM tip. Furthermore, the contribution of the triboelectric effect is quite large when an AFM probe with a large spring constant is used with a large normal force.

## Results and discussion

*Vertically grown ZnO nanorods*

The lengths and diameters of the vertically grown ZnO nanorods, which were measured with a scanning electron microscopy (SEM) system, are shown in

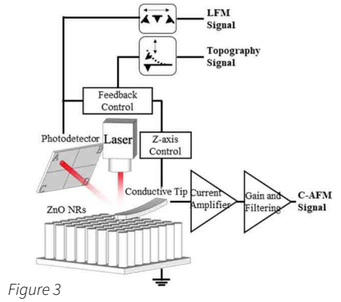


*Figure 3*

Fig. 2. Overall, the aspect ratio of the ZnO nanorods increases with increasing growth time (see Fig. 2d).

Growth of ZnO nanorod samples. (a) Top view and (b) side view of vertically grown ZnO nanorods (S18) and (c) lengths and diameters and (d) aspect ratios of five ZnO nanorod samples (S6–S30). As the growth time increased, both the length and diameter continuously increased. (a) and (b) were obtained using the scanning electron microscope.

### Representations of current versus lateral force via scatter plot

As stated previously, the C-AFM and LFM signals were acquired simultaneously as an AFM probe scanned the ZnO nanorods. Whereas the LFM signal was transmitted through the PSPD, the C-AFM signal was obtained via the current amplifier (Fig. 3). Thus, there was no cross-talk between these two distinct signals. In this study, all the C-AFM and LFM measurements were obtained over a 10 μm × 5 μm area, which resulted in 512 × 128 data points. The C-AFM and LFM data points were represented as *c–afmi, jc*-afmi, j and *lfmi, j,* respectively, using matrix notation. As shown in Fig. 4, a scatter plot was used to represent the correlation between these two sets of data visually. The C-AFM signal from n-type ZnO nanorods has a negative value, whereas the LFM signal during the trace and retrace scans is positive and negative, respectively. Thus, |lc-*afmi*, jll|c-afmi, j| and ||*lfmi, j*ll|lfmi, j| were used for the computations and graphical representations for simplicity.

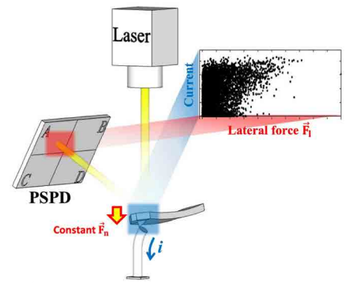


*Figure 4*

Schematic of the experimental setup. Simultaneous acquisition of current and lateral force signals during the scan of vertically grown ZnO nanorods using an AFM probe. The torsional behaviour of the AFM probe was monitored by a laser reflecting from the AFM cantilever into the position-sensitive photodetector. The current signals originating from the ZnO nanorods were detected through the AFM probe and the external circuit with the current amplifier.

Scatter plot of current and lateral force signals. During a typical C-AFM measurement, a constant normal force was applied to the ZnO nanorods. The magnitude of the lateral force applied to the nanorods changed continuously. While completing one raster scan, two sets of C-AFM and LFM signals were simultaneously obtained from every data point on the sample surface. The scatter plot composed of these two distinct signals provides useful information for the mechanism of current generation.

## Conclusions

In this study, we performed comprehensive analysis of the piezoelectric and triboelectric effects generated in ZnO nanorods using an AFM probe. By simultaneously acquiring the C-AFM and LFM signals under a constant normal force, the variations in the ratio of the output current to the applied mechanical force with changes in the aspect ratio of the ZnO nanorods could be observed. In particular, two AFM probes with spring constants of 0.2 and 42.0 N/m were used to investigate the effects of the spring constant on the analysis results. The efficiency of the conversion of the lateral force into the output current was computed, and it was found that the efficiency was enhanced with increasing aspect ratio of the ZnO nanorods. In addition, scatter plots of the current versus the lateral force were produced, and the variations in the patterns of the data points with changes in the aspect ratio were analyzed quantitatively using linear regression. The resulting linear model showed that the slope increased with increasing aspect ratio. This finding indicates that there is a transition of the data points in the scatter plots from the lateral force axis (x-axis) towards the current axis (y-axis) as the aspect ratio increases. The variations in the scatter patterns with changes in the aspect ratio of the ZnO nanorods agreed

with the results of a pixel-wise comparison of the C-AFM and LFM images. It was confirmed that the current signals were contributed by both the piezoelectric and triboelectric effects in a ZnO nanorod. The effect of triboelectricity on the measured current signals was alleviated by reducing a normal force and the spring constant of an AFM probe. This analysis method is expected to be applicable to all freestanding piezoelectric nanomaterials. Furthermore, it is anticipated to facilitate analysis of the effects of the growth conditions of nanomaterials on the efficiency of conversion of the applied mechanical force into the output current.

This article has been condensed under Creative Commons Attribution License. The complete article can be found here: https://go.nature.com/2ZGSoeQ.


## Bringing White Light Interferometry into AFM for semiconductor metrology





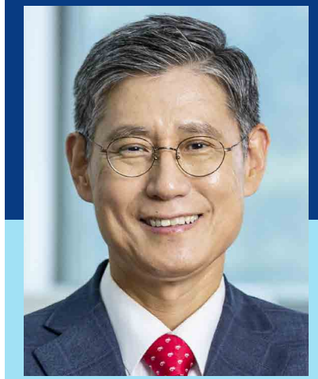

# LET THERE BE LIGHT!

## POWERFUL NEW SEMICONDUCTOR TOOL INTRODUCED BY PARK SYSTEMS COMBINES ATOMIC FORCE MICROSCOPY WITH WHITE LIGHT INTERFEROMETRY

***"Park Systems introduces the Park NX-Hybrid WLI as a powerful semiconductor metrology tool that incorporates the best of AFM and WLI technologies into one seamless system."***

**Dr. Sang-il Park, CEO Park Systems, Inc.**

Park Systems recently announced Park NX-Hybrid WLI, the first fully integrated system that combines Atomic Force Microscopy (AFM) with White Light Interferometer (WLI) profilometry. White light interferometry (WLI) is a nondestructive, non-contact, optical measurement technique used to generate 2D and 3D models of surfaces, and is now widely used for semiconductor production quality assurance. Park Systems introduces the Park NX-Hybrid WLI as a powerful semiconductor metrology tool that incorporates the best of AFM and WLI technologies into one seamless system.

"Park NX-Hybrid WLI introduces a total complementary metrology solution for semiconductor applications requiring both large area scanning and nanoscale metrology," comments Richard Lee, VP of Product Marketing, Park Systems. "The revolutionary design and seamless integration of WLI and AFM emphasizes Park's commitment to provide new, innovative customer driven solutions, as nano metrology requirements for device manufacturing continue to increase." The Park AFM in the integrated system is based on the Park NX-Wafer, the industry leading automated atomic force microscopy system for semiconductor and related devices manufacturing, in-line quality assurance, and research and development. The combined AFM/WLI system provides high throughput imaging over a very large area with the WLI module, and nanoscale metrology with sub-angstrom height resolution over the areas of interest using AFM. Defects of a patterned structure can be detected by comparing images of reference and target sample areas using high speed "hot spot detection", a technique that enables fast localization of defect sites for high resolution AFM review.

The Park WLI module supports both White Light Interferometry and Phase Shifting Interferometry (PSI) modes. The PSI mode is enabled by a motorized filter changer that allows the two objective lenses to be replaced automatically. The Park NX-Hybrid supports objective lens magnification of 2.5x, 10x, 20x, 50x and 100x, featuring a CMOS camera.

Fusing the two complementary techniques, Park NX-Hybrid WLI is a comprehensive automated metrology system, providing substantial cost savings over two separate systems.

"Unlike legacy standalone WLI and AFM systems, Park NX-Hybrid WLI accomplishes more, in a seamless manner, at drastically lower cost of ownership, creating a completely holistic integrated tool," comments Byoung-Woon Ahn, VP of Nanotechnology R&D, Park Systems. "With both tools on the same mount and fed by one EFEM, the system creates fully integrated and exchangeable data, reducing the "fab footprint" and increasing throughput over a larger area."

Park NX-Hybrid WLI was developed for use in applications requiring much higher resolution and accuracy beyond the capability of WLI alone, such as advanced chemical mechanical polishing (CMP) metrology and monitoring, dishing, erosion, and edge-over-erosion (EOE), film thickness, pillar height, hole structure and die to die comparison. It will also be useful in advanced packaging applications including through-silicon via (TSV) and micro bump measurement redistributed layer (RDL) measurement and photo resist residue detection. is a publicly traded corporation on the Korea Stock Exchange (KOSDAQ) with corporate headquarters in Suwon, Korea, and regional headquarters in Santa Clara, California, USA, Mannheim, Germany, Paris France, Beijing, China, Tokyo, Japan, Singapore, India, and Mexico City, Mexico.


# Park FX40

## A Groundbreaking New Class of AFM

### The Autonomous Atomic Force Microscope

Built-in Intelligence - It does all your set up and scanning so that you can focus on your research.

parksystems.com/fx40

SCAN ME!
Watch the video

Park
SYSTEMS